Physical processes in fusion welding

T. DebRoy

Department of Materials Science and Engineering, The Pennsylvania State University, University Park, Pennsylvania 16802

S. A. David

Metals and Ceramics Division, Oak Ridge National Laboratory, Oak Ridge, Tennessee 37831

In recent years, major advances have taken place in our understanding of welding processes and welded materials. Because of the complexity of fusion welding processes, solution of many important contemporary problems in fusion welding requires an interdisciplinary approach. Current problems and issues in fusion welding are reviewed. Solution of these problems, apart from being a contribution to the advancement of science, is also necessary for science-based tailoring of composition, structure, and properties of the welded materials.

CONTENTS

I. INTRODUCTION

Fusion welding of metals and alloys is widely used in the construction of buildings and bridges, and in the shipbuilding, aerospace, automotive, chemical, petrochemical, electronic, and power generation industries. In the United States, welding is utilized in fifty percent of the industrial, commercial, and consumer products that make up the gross national product (Am. Welding Soc., 1992). Since welding is extensively used in the construction industry and since losses of life and property are sometimes traced to defective welds, welding is viewed by many as a primitive science. Nothing can be further from the truth. Major advances have taken place in welding science and technology in the last few decades. In recent years welding has evolved from almost an empirical art to a major interdisciplinary technical activity requiring synthesis of knowledge from various disciplines (David and DebRoy, 1992; David *et al.*, 1994).

In fusion welding, parts are joined by melting and subsequent solidification of adjacent areas of two parts. Welding may be performed with or without the addition of a filler metal. Depending on the thickness of the part, the weld may consist of one or more individual beads formed by each pass of the heat source along the joint. Fusion welding processes are classified according to the nature of the heat source. An electric arc is used in gas-metal arc welding (GMAW), gas-tungsten arc welding (GTAW), and submerged arc welding (SAW). In laser and electron-beam welding, very high-energy-density beams are used as an energy source. Resistive heating is utilized in the electroslag welding process.

Figure 1 is a schematic diagram of the fusion welding process. Three distinct regions in the weldment are clearly observed: the fusion zone, which undergoes melting and solidification, the heat-affected zone, which experiences significant thermal exposure and may undergo solid-state transformation, but no melting, and the base-metal zone, which is unaffected by the welding process.

The interaction of the material and the heat source leads to rapid heating, melting, and vigorous circulation of the molten metal driven by buoyancy, surface tension, impingement or friction, and, when electric current is used, electromagnetic forces. The resulting heat transfer

 0034-6861/95/67(1)/85(28)/$11.20

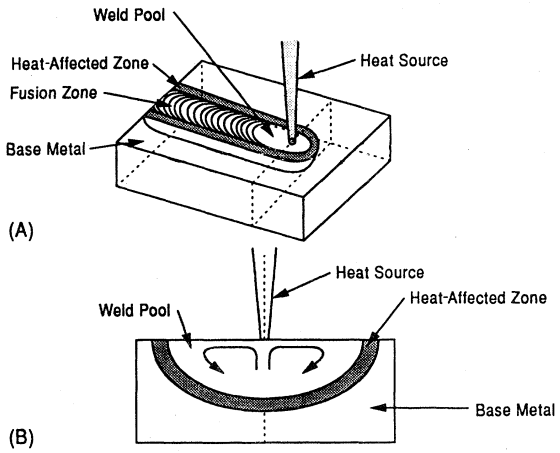

FIG. 1. Schematic diagram of the fusion welding process: (a) interaction between the heat source and the base metal; (b) transverse section (from David and DebRoy, 1992).

and fluid flow affect the size and shape of the weld pool, the cooling rate, and the kinetics and extent of various solid-state transformation reactions in the fusion zone and heat-affected zone. The weld geometry influences dendrite and grain growth selection processes. Both the partitioning of nitrogen, oxygen, and hydrogen between the weld pool and its surroundings, and the vaporization of alloying elements from the weld-pool surface greatly influence the composition and the resulting microstructure and properties of the weld metal. In many processes, such as the arc welding and laser-beam welding, an electrically conducting, luminous gas plasma forms near the weld pool. In welding, the luminosity of the plasmas is a very important property. The light emission from the plasma is a useful feature for monitoring metal-vapor emissions from the weld pool (Bennett and Mills, 1974; Metcalfe and Quigley, 1977; Mills, 1977; Chennat and Albright, 1985; Dunn *et al.*, 1986), which is important for health and environmental safety. In addition, the optical data have been used to estimate the energy reaching the workpiece in laser welding (Collur and DebRoy, 1987; Rockstroh and Mazumder, 1987; Miller and DebRoy, 1990), to calculate the electrical conductivity of the arc in gas-tungsten arc welding (Dunn and Eagar, 1986), and to develop correlations to estimate weld penetration (Dixon and Lewis, 1985).

Since the composition, structure, and properties of the weld metal are affected by widely diverse physical processes, improvements in the weld-metal performance based on science will require an interdisciplinary approach. This article reviews important advances in the understanding of physical processes in welding, including the evolution of weldment structure and properties.

II. HEAT TRANSFER AND FLUID FLOW

A. Energy absorption

During welding, the workpiece absorbs only a portion of the total energy supplied by the heat source. The absorbed energy is responsible for the outcome of the welding process. The consequence of the absorbed energy include formation of the liquid pool, establishment of the time-dependent temperature field in the entire weldment, and the structure and properties of the weldment. Therefore it is very important to understand the physical processes in the absorption of energy during the welding processes. The physical phenomena that influence the energy absorption in the workpiece are unique to each welding process. For a given power source, the extent of the energy absorbed by the workpiece depends on the nature of the material, the type of the heat source, and the parameters of the welding process.

For arc welding, the fraction of the arc energy transferred to the workpiece, η, commonly known as the arc efficiency, is given by (Lancaster, 1980)

$$\eta=\frac{q}{VI}=1-\frac{q_e+(1-n)q_p+mq_w}{VI}\ , \tag{1}$$

where q is the rate of heat absorption by the workpiece, I and V are the welding current and voltage, respectively, q_e is the rate of heat transfer to the electrode from the heat source, q_p is the energy radiated and convected to the arc column per unit time, of which a proportion n is transferred to the workpiece, and q_w is the rate of heat absorbed by the workpiece, of which a proportion m is radiated away. For a consumable electrode, the amount of energy transferred to the electrode is eventually absorbed by the workpiece. Thus Eq. (1) can be simplified to

$$\eta=1-\frac{(1-n)q_p+mq_w}{VI}\ . \tag{2}$$

Equations (1) and (2) are useful in understanding how the various types of heat loss affect arc efficiency. However, it is difficult to estimate the heat-loss terms q_e, q_p, and q_w accurately from theoretical considerations. Therefore, as a practical matter, the arc efficiency is determined experimentally by doing an appropriate calorimetric or other measurement of the heat received by the workpiece for a given welding condition (Smartt *et al.*, 1985; Giedt *et al.*, 1989; Fuerschbach and Knorovsky, 1991). Arc efficiencies in the range of 20 to over 95 % have been reported (Kou, 1987).

During laser welding, the absorption of the laser beam by the workpiece is affected by several factors such as the wavelength of the laser, the nature of the surface, joint geometry, and the size and nature of the plasma present above the weld pool. The absorption of infrared energy by metals depends largely on conductive absorption by free electrons. Therefore, for clean metal surfaces, the absorptivity can be calculated from the knowledge of the electrical resistivity of the substrate. Arata and Miyamoto (1978) demonstrated that the absorptivity of various flat, polished surfaces is a linear function of the square root of the electrical resistivity of the respective metals based on experimental data. Bramson (1968) related the absorptivity to the substrate resistivity and the wave-

length of the laser radiation:

$$\eta(T)=0.365\left[\frac{r}{\lambda}\right]^{1/2}-0.0667\left[\frac{r}{\lambda}\right]+0.006\left[\frac{r}{\lambda}\right]^{3/2}, \tag{3}$$

where $\eta(T)$ is the absorptivity at a temperature T, r is the resistivity in Ω cm, and λ is the wavelength in cm. Such calculations are accurate for clean surfaces of the metal and when a plasma plume does not affect the absorption of the laser beam. All metal surfaces are highly reflective to the infrared radiation of a CO_2 laser at room temperature, and thus the transfer of energy from the laser beam to the workpiece can be inefficient. When the power density is high, material can vaporize rapidly from the molten pool, and a cavity of the shape of a keyhole can form in the material because of the recoil force of the vapor on the liquid metal. When the keyhole forms, the energy absorption efficiency can improve dramatically, to a value much higher than that predicted by Eq. (3), owing to multiple reflections of the beam in the cavity.

When a plasma forms near the weld pool, a part of the laser-beam energy can be absorbed by the plasma before the beam reaches the material. Thus it is important to know how much of the laser energy is actually absorbed by the plasma. Theoretical treatments are available for simple systems (ZelDovich and Raizer, 1966). A free electron traveling through the electric field in a plasma can absorb a photon and acquire additional kinetic energy.[1] The free-free transition involving photon absorption is called inverse bremsstrahlung. ZelDovich and Raizer (1966) obtained the following bremsstrahlung absorption coefficient assuming the electron velocities obey a Maxwell distribution:

$$k_v=3.69\times10^8\frac{Z^2}{\nu^3\sqrt{T}}N_+N_e\ , \tag{4}$$

where k_v is the absorption coefficient for energy absorption by plasma, Z is the ionic charge, ν is the frequency, T is the electron temperature, and N_+ and N_e are the number densities of positively charged ions and electrons, respectively. Considering CO_2 laser radiation of 10.6 μm wavelength and singly charged species, and taking $N_+=N_e$ to satisfy electroneutrality of plasma, the equation can be simplified to (Collur, 1988)

$$k_v=1.63\times10^{32}(N_e)^2/\sqrt{T}\ . \tag{5}$$

Equation (5) has been used for the determination of the spatial variation of the absorption coefficient from the optical emission data (Collur, 1988). During welding, the intensity of light emission versus wavelength data are obtained using an appropriate system usually consisting of a fiber-optic cable, a light detector, the necessary electronic equipment for digitizing the optical signal, and a host computer with appropriate software for data storage and analysis. A typical spectrum, shown in Fig. 2, was recorded for pulsed CO_2 laser welding of a stainless steel. The intensity peaks corresponding to iron, manganese, and chromium emissions are observed. The electron temperature T and number density n_e necessary for the determination of the absorption coefficient, are obtained from the intensity versus wavelength data. Determination of electron temperatures requires monitoring of at least two appropriate peaks (Shaw, 1975; Key, McIlwain, and Isaacson, 1980; Key, Chan, and McIlwain, 1983). The accuracy of temperature measurement can be greatly improved when data for several peaks are used (Glickstein, 1976; Knudtsen *et al.*, 1987; Peebles and Williamson, 1987; Collur and DebRoy, 1989; Miller and DebRoy, 1990). Procedures for the determination of electron temperature and electron density are available in standard textbooks (Griem, 1964, 1974; Heald and Wharton, 1965; Boumans, 1966).

Rockstroh and Mazumder (1987) conducted aluminum welding experiments using argon shielding gas. They found that the extent of inverse bremsstrahlung absorption was about 20% and 31% for welding with 5 and 7 kW laser powers, respectively. For welding of steels with low-power CO_2 lasers, overall bremsstrahlung absorptions of less than 10% have been reported by Collur (1988) and Miller (1989). At a given position within the plasma, the extent of absorption of the laser beam depends on the local properties of the plasma. The local values of the intensities are obtained from the experimentally determined line-of-sight intensities by a suitable deconvolution scheme such as the Abel transformation

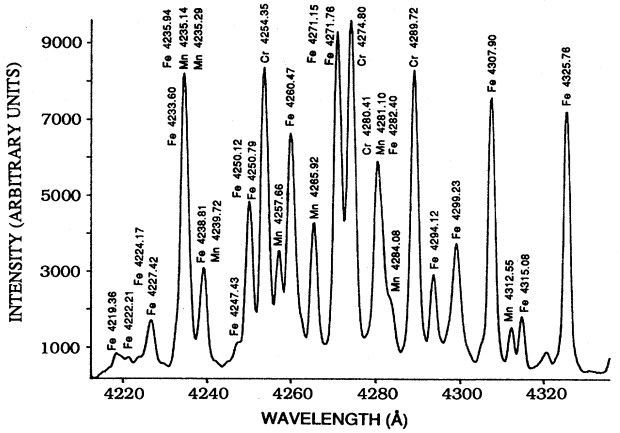

FIG. 2. A typical spectrum recorded during pulsed carbon dioxide laser welding of AISI 201 grade stainless steel (0.10% C, 6.1% Mn, 16.3% Cr, 5.47% Ni, 0.46% Si, 0.33% Cu, 0.25% Mo in iron) using a pulsed CO_2 laser operated at 100 Hz with 3 ms pulse length, 4×10^6 W/cm^2 peak power, and 5 mm/sec welding speed (Miller and DebRoy, 1990).

[1]The absorption of light can also occur when an electron passes through the field of a neutral atom. In contrast to the field of an ion, the field of a neutral atom decreases rapidly with distance, and therefore the electron must pass very closely to the atom to ensure absorption of photons. For this reason, the absorption effect is significantly more pronounced in a plasma than in a molecular gas.

(Barr, 1962; Rockstroh, 1987; Collur, 1988). The values of the absorption coefficient vary significantly with location, and the loss of laser-beam energy is more pronounced close to the surface of the workpiece. Therefore the estimation of the overall extent of the absorption is not straightforward, and extensive calculations are required for the estimation (Miller and DebRoy, 1990). The available data show that the beam absorption by the plasma is significant under welding conditions, and that absorption must be considered to quantitatively understand heat transfer in welding processes.

In the case of laser welding, the amount of energy absorbed by the plasma and the workpiece can be estimated theoretically, at least in principle. However, theoretical calculations may be inaccurate in many cases. For example, in the case of laser welding, theoretically estimated absorption coefficients obtained from relations such as Eq. (3) are valid for flat surfaces. Workpiece surfaces are rarely optically flat. Furthermore, when the weld pool forms, the liquid surface may deform because of the motion of the liquid and/or the inherent instability of the flow. In addition, the calculations are valid for pure metal surfaces. Most metal and alloy surfaces have thin layers of oxides, which can have a significant effect on the absorption coefficient. In the keyhole mode of welding, theoretical estimations of the absorption coefficient depend on the depth of the keyhole. In practice, the depth of the keyhole is difficult to determine. Similarly, quantitative calculation of bremsstrahlung absorption coefficients is a highly complex task, since it requires estimation of the properties of the welding plasma during laser welding. The properties of welding plasma vary significantly depending on the welding conditions and the material welded. Thus it is time consuming and difficult to obtain the data necessary for the calculation of the bremsstrahlung absorption coefficient. Because of the difficulties in the accurate theoretical prediction of the absorption coefficient under welding conditions, experimentally determined values should be used where such data are available (Huntington and Eagar, 1983; Khan and DebRoy, 1985; Fuerschbach, 1994). However, when experimental data are not available, Eqs. (3) to (5) can be used to estimate the energy absorbed by the workpiece and the plasma.

B. Fluid flow in the weld pool

1. Driving forces

The properties of the weld metal are strongly affected by the fluid flow and heat transfer in the weld pool. The flow is driven by surface tension, buoyancy, and, when electric current is used, electromagnetic forces (Kou and Le, 1983; Chan *et al.*, 1984; Oreper and Szekely, 1984; Dowden *et al.*, 1985; Paul and DebRoy, 1986; Tsai and Kou, 1989; Zacharia *et al.*, 1989a, 1989b; Mazumder and Kar, 1992; Mundra and DebRoy, 1993b, 1993c; Choo and Szekely, 1994). In some instances, aerodynamic drag forces of the plasma jet may also contribute to the convection in the weld pool (Matsunawa, 1993). Buoyancy effects originate from the spatial variation of the liquid-metal density, mainly because of temperature variations, and, to a lesser extent, from local composition variations. Electromagnetic effects are a consequence of the interaction between the divergent current path in the weld pool and the magnetic field that it generates. This effect is important in arc and electron-beam welding, especially when a large electric current passes through the weld pool. In arc welding, a high velocity plasma stream impinges on the weld pool. The friction of the impinging jet on the weld-pool surface can cause significant fluid motion. Fluid flow and convective heat transfer are often very important in determining the size and shape of the weld pool, the weld macro and microstructures, and the weldability of the material.

2. Marangoni Force

The spatial gradient of surface tension is a stress, known as the Marangoni stress. The spatial variation of the surface tension at the weld-pool surface may arise owing to variations of both temperature and composition. Frequently the main driving force for convection is the spatial gradient of surface tension at the weld-pool surface. In most cases, the difference in surface tension is due to the temperature variation at the weld-pool surface. For such a situation, the Marangoni stress can be expressed as

$$\tau = \frac{d\gamma}{dT}\frac{dT}{dy} , \tag{6}$$

where τ is the shear stress due to temperature gradient, γ is the interfacial tension, T is the temperature, and y is the distance along the surface from the axis of the heat source. If a boundary layer develops, the shear stress τ can also be expressed as (Geankoplis, 1983)

$$\tau = \frac{0.332\rho^{1/2}\mu^{1/2}u^{3/2}}{y^{1/2}} , \tag{7}$$

where ρ and μ are the density and viscosity, and u is the local velocity. An order of magnitude calculation of the maximum velocity u_m, can be done by combining Eqs. (6) and (7), and by assuming that the maximum velocity occurs at a location approximately halfway between the heat-source axis and the weld-pool edge, i.e., at $y = W/4$, where W is the width of the weld pool:

$$u_m^{3/2} \approx \frac{d\gamma}{dT}\frac{dT}{dy}\frac{W^{1/2}}{0.664\rho^{1/2}\mu^{1/2}} . \tag{8}$$

For a typical value of pool width of 0.5 cm, metal density of 7.2 gm/cm^3, viscosity of 0.06 poise, temperature coefficient of surface tension $(d\gamma/dT)$ of 0.5 dynes/(cm °C), and spatial gradient of temperature of 600 °C/cm, the maximum velocity is approximately 62 cm/sec. Considering that this weld pool is only 0.5 cm wide, this velocity is rather large. Computed values of

the order of 100 cm/sec have been reported in systems dominated by Marangoni convection (Szekely, 1986; Paul and DebRoy, 1988). When the velocities are small, the shear stress τ, cannot be accurately estimated by Eq. (7), which is based on the boundary layer theory. For such a situation, a rough estimate of the shear stress can be obtained from geometric consideration as $2\mu u_m/d$, where d is the depth of the weld pool. The expression for the approximate value of the maximum velocity can be obtained by combining this expression for shear stress with the expression for Marangoni stress, i.e., Eq. (6):

$$u_m \approx \frac{d}{2\mu}\frac{d\gamma}{dT}\frac{dT}{dy} . \tag{9}$$

The velocities calculated from Eqs. (8) and (9) can provide a rough idea of the flow of liquid metal in the weld pool. Detailed solutions of the equations of conservation of mass, momentum, and heat are necessary for the calculation of temperature and velocity fields in the weld pool.

3. Buoyancy and electromagnetic forces

When the surface-tension gradient is not the main driving force, the maximum velocities can be much smaller. For example, when the flow occurs owing to natural convection, the maximum velocity u_m can be approximated by the following relation (Szekely, 1986):

$$u_m \approx \sqrt{g\beta\Delta T d} , \tag{10}$$

where g is the acceleration due to gravity, β is the coefficient of volume expansion, ΔT is the temperature difference, and d is the depth. For the values of $\Delta T = 600\,^{\circ}\mathrm{C}$, $g = 981$ cm/sec^2, $\beta = 3.5\times10^{-5}/^{\circ}\mathrm{C}$, and $d = 0.5$ cm, the value of u_m is 3.2 cm/sec. The existence of electromagnetically driven flow was demonstrated by Woods and Milner (1971), who observed flow of liquid metal when current was passed in the metal bath by means of a graphite electrode. In the case of electromagnetically driven flow in the weld pool, the velocity values reported in the literature are typically in the range of 2 to 20 cm/sec (Wang and Kou, 1986). The magnitude of the velocities for both buoyancy and electromagnetically driven flows in the weld pool are commonly much smaller than those obtained for surface-tension-driven flows.

4. Critical issues in flow calculations

Calculations of fluid flow and heat transfer in the weld pool are now routinely performed through numerical solution of the equations of conservation of mass, heat, and momentum. These calculations have provided detailed insight about welding processes that could not have been achieved otherwise.

Because the welding processes are highly complex, a fully comprehensive modeling of weld-pool heat transfer and fluid flow requires extensive calculations. Consequently, one has to judge the extent of simplification that can be tolerated for a particular application. Three-dimensional versus two-dimensional simulations, transient versus steady state, flat weld-pool surface versus free-deformable surface, and laminar structure of flow in the weld pool versus turbulent flow simulated using turbulence models of different degrees of sophistication are a selection of the available choices. While it is expedient to weigh heavily in favor of a particular set of simplifications because of the availability of an existing software package, or other computational conveniences, the consequences of such choices vary, depending on the goals of the simulation effort. Mathematical modeling is a powerful tool for understanding the development of weld-pool geometry and other welding parameters. However, in view of the complexities of the welding processes, attempts to understand welding processes through simulation must involve concomitant well-designed experimental work to validate the models.

A more fundamental limitation of the theoretical calculations is imposed by the lack of necessary thermophysical data. Our existing data base of high-temperature materials' properties was developed, to a large extent, to understand the manufacturing and the subsequent processing or use of metals and alloys. Unlike welding, other materials processing operations seldom involve temperatures much above the melting point of metals. Furthermore, in most processing operations, the processing environment does not contain plasma. In contrast, in many welding operations, the peak temperature in the weld pool can reach close to the boiling point of the metal, and a plasma plume often surrounds the weld metal. Thermophysical data for such high-temperature systems are scarce, especially for systems containing plasma. Thus, apart from the difficulty in adapting rigorous simulation of the highly complex welding process, an in-depth understanding of the behavior of the welding process is often impeded by the lack of appropriate thermophysical data.

Although the methodologies of flow calculations are now well accepted, and reliable commercial computer programs for the solution of the equations of conservation of mass, heat, and momentum have been adapted for the calculation of weld-pool fluid flow to achieve high efficiency and accuracy of the numerical scheme, inaccuracies in the computed velocities result from several sources. First, the presence of some impurities on the surface are known to lower the impact of the surface-tension-driven flow. For example, Woods and Milner (1971) demonstrated Marangoni flow in a mercury bath contained in a flask under vacuum. However, when air was introduced into the flask, no liquid motion took place. The observation was attributed to the oxygen contamination of the mercury surface. Thus, in some cases, the spatial gradient of surface tension[2] for pure metals

[2]The spatial gradient of surface tension is the product of spatial gradient of temperature and the slope of the surface tension versus temperature plot (surface-tension gradient with respect to temperature).

and alloys, assumed in the calculations, may be significantly different from the actual value for the real metals and alloys under the welding conditions. Second, the value of the viscosity used in the solution of the equations of conservation of momentum can be higher than the molecular viscosity in many cases. This is because an enhanced viscosity is consistent with high-momentum transport rates resulting from large fluctuating velocities that are inevitable when very strong recirculation occurs in relatively small weld pools. Contemporary calculations of velocities in systems with large fluctuating velocities are based on the available turbulence models, which contain several empirical constants determined from parabolic flows in large systems. How the large recirculating velocities in small scale welding systems affect the extent of enhancement of the heat, mass, and momentum-transfer rates is not well understood. In some previous works, enhanced viscosities and thermal conductivities have been used to address the problem (Paul and DebRoy, 1986, 1988; Choo and Szekely, 1994). Finally, only a limited amount of data are available (Sahoo and DebRoy, 1987) on the effect of plasma in influencing the temperature dependence of surface tension. In the calculations of Marangoni convection, the inaccuracies in the available surface tension versus temperature data lead to errors in the computed velocities.

Marangoni convection in weld pools is now widely accepted to be a major driving force for fluid flow in the weld pool. However, the experimental observations of Woods and Milner (1971) and other considerations discussed in this section indicate that the exact values of the calculated velocities may not always be attainable under practical welding conditions. Consequences of such uncertainties of the calculated velocities on the temperature fields vary, depending on the relative importance of conduction and convection in the overall heat transfer. Trends in the computed velocities as a function of a welding variable such as the heat-source intensity are more dependable than the exact computed velocity field values under a given set of welding conditions. Detailed experimental determination of the flow velocities in the weld pool remains a major challenge in the field (Mazumder, 1993). In the absence of adequate experimental work, contemporary literature relies heavily on the available recourse of numerical calculations to obtain insight about weld-pool heat transfer and fluid flow.

Process models are an important component in achieving effective automation in welding processes. The comprehensive phenomenological models, embodying detailed description of the important physical processes in welding, cannot be used for real-time welding applications, since they require extensive computer time. However, large phenomenological models can be used to calibrate and verify relatively simple process models, such as neural networks (Anderson *et al.*, 1993; White *et al.*, 1993), which do not consider any of the physical processes in welding and, as a consequence, are computationally simple and can be used in real time.

C. Relative importance of conduction and convection

The relative importance of conduction and convection in the overall transport of heat in the weld pool can be assessed from the value of the Peclet number Pe which is given by

$$\mathrm{Pe}=\frac{u\rho c_p L}{k}\ , \tag{11}$$

where u is the velocity, ρ is the density, c_p is the specific heat at constant pressure, L is the characteristic length, and k is the thermal conductivity of the melt. For a typical case with $u=10$ cm/sec, $\rho=7.2$ gm/cm^3, $c_p=0.2$ cal/(gm °C), $L=0.5$ cm, and $k=0.1$ cal/(cm sec °C), the Pe is 72. When the Peclet number is much larger than one, heat transport occurs primarily by convection, and heat conduction in the weld pool is not important. However, for metals with high thermal conductivities, at low velocities and for small pool size, the value of Pe can be low (Pe $\ll 1$), and accurate calculations of heat transfer can be done using relatively simple conduction calculations. It should also be noted that the conduction of heat in the solid region is very important for the dissipation of heat away from the weld pool. Therefore the thermal conductivity of the solid and the specimen dimensions are very important in determining the size of the molten pool.

D. Convection effects on weld-pool shape and size

Variable depth of penetration during the welding of different batches of a commercial material with compositions within a prescribed range has received considerable attention. Often, the penetration depth is determined by the concentration of surface-active elements such as oxygen or sulfur in steels (Heiple and Roper, 1982a, 1982b; Heiple *et al.*, 1982; Paul and DebRoy, 1988). These elements can affect the temperature coefficient of surface tension, $d\gamma/dT$, the resulting direction of convective flow in the weld pool (Paul and DebRoy, 1988), and the shape of the weld pool. The interfacial tension in these systems could be described by a formalism based on the combination of Gibbs and Langmuir adsorption isotherms (Sahoo, DebRoy, and McNallan, 1988; McNallan and DebRoy, 1991):

$$\gamma=\gamma_m^0-A(T-T_m)-RT\Gamma_s\ln(1+k_1a_ie^{-\Delta H^0/R'T}) \tag{12}$$

where γ is the interfacial tension as a function of composition and temperature, γ_m^0 is the interfacial tension of the pure metal at the melting point T_m, A is the temperature coefficient of surface tension for the pure metal, R and R' are the gas constants in appropriate units, T is the absolute temperature, Γ_s is the surface excess of the solute at saturation solubility, k_1 is the entropy factor, a_i is the activity of the solute, and ΔH^0 is the enthalpy of segregation. The calculated values of surface tension

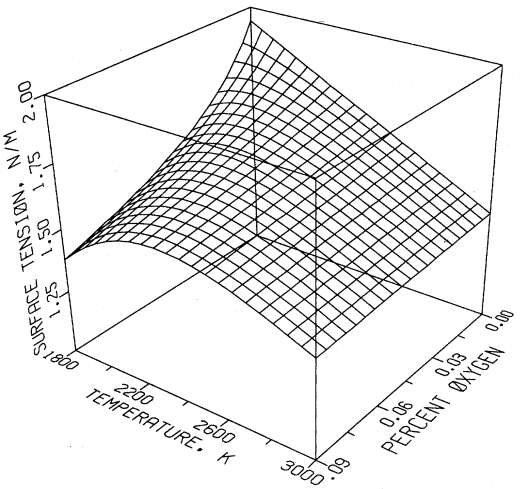

FIG. 3. Surface tension of iron-oxygen alloys as a function of temperature and oxygen concentration (DebRoy, 1993b).

(Sahoo, DebRoy, and McNallan, 1988; Mundra and DebRoy, 1993a) for Fe-O alloys are presented in Fig. 3. It is observed that for certain concentrations of oxygen, $d\gamma/dT$ can change from a positive value at "low" temperature to a negative value at "high" temperature. This implies that in a weld pool containing fairly high oxygen contents, $d\gamma/dT$ can go through an inflection point on the surface of the pool. Under these conditions, the fluid flow in the weld pool is more complicated than a simple recirculation.

The calculated GTAW fusion-zone profiles (Mundra and DebRoy, 1993a) for pure iron, and an iron − 0.03 wt. % O alloy are presented in Fig. 4. The results clearly show the significant effect of oxygen concentration on the

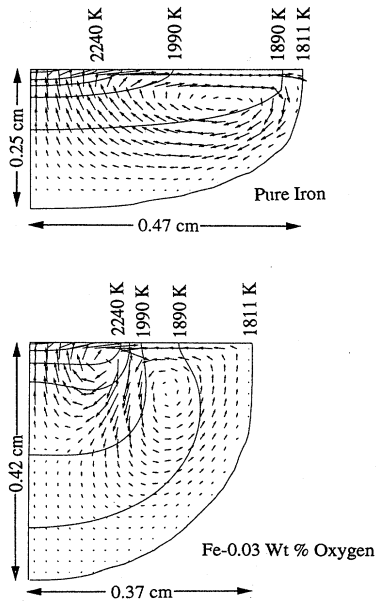

FIG. 4. Velocity and temperature fields for the welding of pure iron, and iron with 0.03 wt. % oxygen (DebRoy, 1993b).

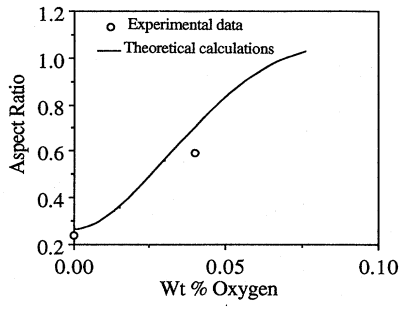

FIG. 5. Comparison of the predicted and experimental aspect (depth-to-width) ratios (DebRoy, 1993). The oxygen concentration of 0.04 wt. % is obtained from the Cr—O equilibrium data of Richardson (1974) for 21 % Cr.

weld-pool shape and the aspect ratio. Near the heat source, where the temperature is very high, the flow is radially outward. However, a short distance away from the heat source, where the temperature drops below the threshold value for the change in the sign of $d\gamma/dT$, the flow reverses in direction. The flow field is not a simple recirculation. The computed values of the aspect ratio are compared with the experimental data of Heiple and Roper (1982b) in Fig. 5. Good agreement is achieved between the calculated results and the experimental data. A similar behavior was also observed (Zacharia *et al.*, 1989a) for the GTAW fusion welding of 304 stainless steel containing sulfur. Apart from the good agreement between the experimental and the calculated weld-pool shapes, the calculations reveal new insight about the complexity of the flow field. Although the qualitative effects of the role of surface-active elements are known, the numerical calculations provide a basis for quantitative assessment of their role in the development of the weld-pool geometry.

E. Simple features of solidification structure

The cooling rate at a given solidification front location is the product of the temperature gradient and the solidification growth rate. For several alloys, the secondary dendrite arm spacings in the newly formed solid have been experimentally correlated with the cooling rates. Therefore, using numerically computed cooling rates and the available experimental correlation, the secondary dendrite arm spacing can be estimated. The experimental correlations between secondary dendrite arm spacing and the cooling rate obtained by Abdulgadar (1988) and Brower *et al.* (1970) are shown in Fig. 6. Paul and DebRoy (1988) calculated cooling rates at the edge of the weld pool from the numerical calculations of convective heat transfer. These cooling rates were used to determine the secondary dendrite arm spacings. For example, secondary dendrite arm spacings of 0.9 and 0.4 μm were obtained for computed cooling rates for 5 and 31 mm/sec welding speeds, respectively. These values

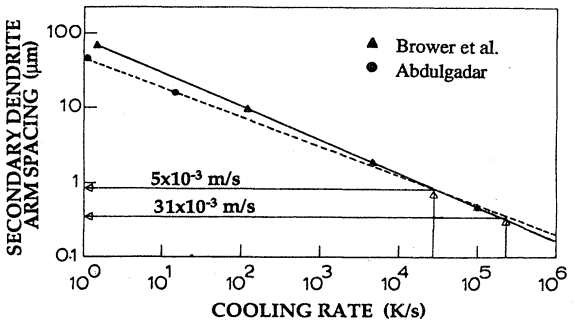

FIG. 6. Plot of secondary dendrite arm spacing as a function of cooling rate for conduction mode laser welding of AISI 201 stainless steel (Paul and DebRoy, 1988).

were in good agreement with the experimental results of Paul and DebRoy (1988). The agreement between the predicted secondary dendrite arm spacing and the values obtained from independent data demonstrates that the calculated values of cooling rates are fairly accurate. In another investigation (Zacharia *et al.*, 1989b) of the effect of pulsed laser welding on the thermal response of 310 and 316 austenitic stainless steels, the cooling rates were theoretically calculated from fundamental principles of transport phenomena. The secondary dendrite arm spacings were determined from the microstructures. The results indicated excellent agreement between the measured and the expected secondary dendrite arm spacings based on the cooling rates. The investigations with both continuous (Paul and DebRoy, 1988) and pulsed (Zacharia *et al.*, 1989b) heat sources indicate that simple features of the solidification structure can be determined from the available numerical models of weld-pool transport phenomena.

III. VAPORIZATION FROM WELD-POOL SURFACE

A. Weld-metal composition change

The weld-pool surface temperatures are normally much higher than the melting points of the weld metals. Consequently, pronounced vaporization of alloying elements takes place, especially when high-energy-density heat sources are used (Block-Bolten and Eagar, 1984; Khan and DebRoy, 1984; Blake and Mazumder, 1985; Collur *et al.* 1987; Cieslak and Fuerschbach, 1988; Khan *et al.*, 1988). Such losses often result in a change in the composition of the weld metal, affect weld properties, and are a serious problem in the welding of many important engineering alloys. Weld-metal composition changes (Collur *et al.*, 1987) due to laser welding of thin samples of various grades of high-manganese stainless steels are indicated in Fig. 7. The severe depletion of manganese in the weld zone in each case is clearly evident. From mass balance, the decrease in the concentration of manganese, $\Delta\%\mathrm{Mn}$, can be expressed as follows:

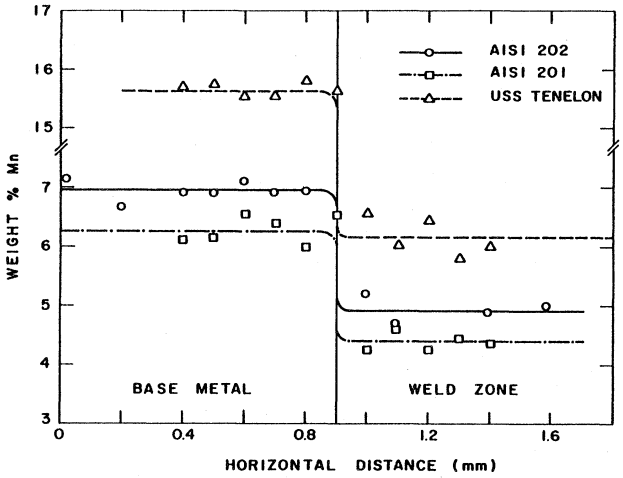

FIG. 7. Concentration of manganese vs distance in the base metal and in the weld zone for continuous wave carbon dioxide laser welding; Laser power, 560 watts; welding speed, 3.5×10^{-3} m/sec; shielding gas flow rate, 10^{-4} m^3/sec; sample thickness, 7×10^{-4} m (Collur *et al.*, 1987).

$$\Delta\%\mathrm{Mn}=\frac{100 r_{\mathrm{Mn}}}{\rho}\left[\frac{A}{v}\right], \tag{13}$$

where r_{Mn} is the vaporization rate of manganese per unit surface area, A is the weld-pool surface area, ρ is the density of the weld metal, and v is the volume of the weld metal melted per unit time. The weld-metal composition change depends on the vaporization flux and the surface-to-volume ratio of the weld pool, with the latter often being the dominant factor. For the conditions of the experiments presented in Fig. 7, a small weld pool having a width of less than a millimeter was formed, and a significant composition change was observed.

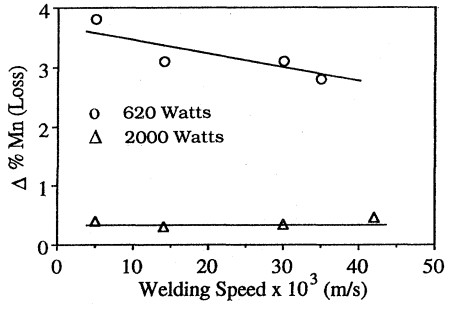

FIG. 8. Effect of welding speed and power on the decrease in the manganese concentration of stainless steels resulting from laser welding. The symbol $\Delta\%$ Mn represents the difference between the manganese concentration in the base metal and the weld metal. Samples of AISI 202 stainless steels were welded with laser power of 620 W, and AISI 201 samples were welded with laser power of 2000 W (DebRoy, 1993a, 1993b, based on the data in Khan, 1987).

An increase in the power of the heat source does not result in a more pronounced composition change. This fact may appear counterintuitive at first. The composition change is most pronounced at low powers because of the small size and, consequently, high surface-to-volume ratio of the weld pool (Khan *et al.*, 1988), as can be observed from Fig. 8.

B. Vapor composition

Khan and DebRoy (1984) determined the relative rates of vaporization of various elements from the weld pool during laser welding of AISI 202 stainless steel. The primary alloying elements in this steel are 7.5% Mn, 17.8% Cr, and 4.7% Ni. A portion of the vaporized material was collected as condensation on the inner surface of a cylindrical quartz tube, with both ends open, which was held stationary and coaxial with the laser beam. From the analysis of the condensed material, they demonstrated that the vapor consisted primarily of iron, manganese, chromium, and nickel. The vapor composition was about the same as what would be expected from the base metal maintained isothermally at its boiling point. It should be noted that for the estimation of temperature, the rates of vaporization of the individual alloying elements are not needed. Since the vaporization rate is a strong function of temperature, they argued that most of the condensate originated from the center of the weld pool near the laser-beam axis where the local temperature was close to the boiling point of the alloy for their experiments. Thus, during welding of alloys with more than one volatile component, the vapor composition may provide important information about the maximum temperature in the weld pool.

C. Evaporation rate calculations

A simple model to calculate evaporation rate is given by the Langmuir equation (Dushman, 1962):

$$J=\frac{p^0}{\sqrt{2\pi MRT}}\,, \tag{14}$$

where J is the vaporization flux in moles/(cm^2 sec), p^0 is the vapor pressure of the vaporizing species over the liquid in gm/(cm sec^2), M is the molecular weight of the vaporizing species in gm/gm mole, R is the gas constant, 8.314×10^7 gm cm^2/(sec^2 gm mole K), and T is the temperature in K. The Langmuir equation can be used to calculate vaporization rates at very low pressure where significant condensation of the vapor does not take place. Experimental data indicate that the vaporization rate under most welding conditions is five to ten times lower than the rate predicted by the Langmuir equation. However, the equation has been used to determine relative rates of vaporization of various alloying elements (Khan and DebRoy, 1984), and sometimes, even in recent literature, to calculate vaporization rates at atmospheric pressure (Metzbower, 1993).

DebRoy *et al.* (1991) developed a comprehensive mathematical model to understand vaporization of pure metals and the loss of alloying elements from stainless-steel weld pools (Mundra and DebRoy, 1993b, 1993c). The calculations involved numerical solution of the equations of conservation of mass, momentum, and translational kinetic energy of the vapor near the weld-pool surface. The fluid flow and heat transfer within the molten pool were simulated by solution of the Navier-Stokes equations and the equation of conservation of energy to determine the temperature distribution at the weld-pool surface. The heat transfer to the shielding gas and the heat loss due to vaporization of the alloying elements were taken into account in the calculations. The computed weld-pool temperature distribution was used for the vaporization rate calculations.

A key feature of the calculations is the consideration of the pressure-gradient-driven mass transfer (Anisimov and Rakhmatulina, 1973; Knight, 1979). In laser processing of metals and alloys, the peak temperature reached at the surface often exceeds the boiling point of the irradiated material. For example, von Allmen (1987) determined molten pool temperatures in excess of the boiling point for laser treatment of copper. Batanov *et al.* (1973) also indicated that temperatures on the surface of a laser irradiated material can be higher than the boiling point. Chan and Mazumder (1987) have also reported computed temperatures greater than the boiling point during laser irradiation of aluminum, titanium, and a superalloy. Theoretical calculations of the vaporization rates by Anisimov and Rakhmatulina (1973) and Knight (1979) are based on the premise that the liquid-pool surface temperatures are higher than the boiling point.

At temperatures higher than the boiling point, the pressures in the vicinity of the pool are greater than the ambient pressure. This excess pressure provides a driving force for the vapor to move away from the surface. To include this effect, the velocity distribution functions of the vapor molecules escaping from the weld-pool surface at various locations, shown schematically in Fig. 9, were used. At the weld-pool surface, the molecules cannot travel in the negative direction, and, as a consequence, the distribution function is half Maxwellian. Close to the weld-pool surface, the velocity distribution reaches the equilibrium Maxwellian distribution in a space of several mean free paths length, known as the Knudsen layer. At the outer edge of this layer, the vapor molecules can have all possible velocities from $-\infty$ to $+\infty$, at least in principle, as observed in Fig. 9. A portion of the vaporized material condenses on the liquid surface. The velocity distribution functions were used in the equations of conservation of mass, momentum, and translational kinetic energy in the gas phase to determine the rates of vaporization from and the rates of condensation on the weld-pool surface owing to a total pressure gradient at the pool surface. In addition, mass transfer rates due to concentration gradients can be determined using correlations that exist between various dimension-

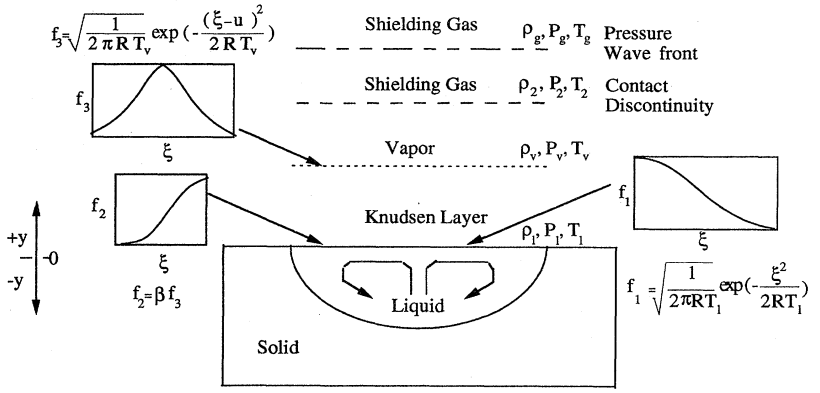

FIG. 9. Schematic diagram of the velocity distribution functions in the Knudsen layer and adjacent regions (DebRoy *et al.*, 1991).

less numbers to include this effect in the overall vaporization rate.

In Fig. 10, the experimentally determined vaporization rates are compared (DebRoy *et al.*, 1991) with the rates computed from the model and the values calculated from the Langmuir equation for pure iron and titanium. It is observed that the experimentally determined vaporization rates are closer to the values predicted by the model than the rates calculated from the Langmuir equation. However, in all cases, the model predictions of the rates are somewhat higher than the corresponding experimentally determined values. The lower experimental rates are consistent with plasma induced suppression of vaporization rates discussed in a previous publication (Sahoo, Collur, and DebRoy, 1988). Similarly, calculated values of vaporization rates during high-power conduction mode CO_2 laser welding of 201 stainless steel, after taking into account the effect of plasma, agree well with the corresponding experimental data as shown in Fig. 11. The calculated vaporization rates are significantly better than the corresponding values obtained from the Langmuir equation, because higher accuracy is achieved by including more realistic and detailed descriptions of the physical processes, and, consequently, by performing more complex calculations.

D. Heat effect of evaporation

Depending on the vaporization rate and the composition of the weld metal, evaporation of alloying elements from the weld-pool surface may lead to significant cooling of the liquid metal in the weld pool (Block-Bolten and Eagar, 1982, 1984; Cieslak and Fuerschbach, 1988; Mundra and DebRoy, 1993b). The effect of the evaporative heat loss in the calculation of peak temperatures for different laser powers is shown in Fig. 12. The computed results show that evaporative heat loss can significantly reduce the peak temperature. The peak temperatures in Fig. 12 decreased slightly with power mainly because of the changes in the beam characteristics at high laser powers. The results indicate that substantial errors in the calculated temperatures may result when the heat loss is ignored (Mundra and DebRoy, 1993b).

Often, the energy necessary for the evaporation of alloying elements from the weld pool is a small fraction of the total energy used in the welding. Block-Bolten and Eagar (1982, 1984) considered the following heat balance for the evaporation of elements to understand the maximum temperature that can be attained during welding:

$$W(T)(L_e-\Delta\bar{H})=xP\ , \tag{15}$$

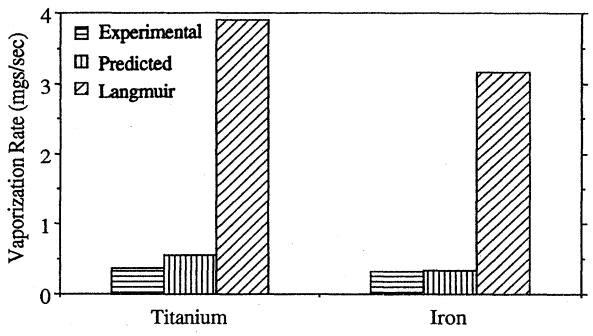

FIG. 10. Comparison of the experimental vaporization rates of pure iron and titanium with the corresponding rates calculated from the Langmuir equation and the model: laser power, 500 W; argon flow rate, 1 l/min (DebRoy *et al.*, 1991).

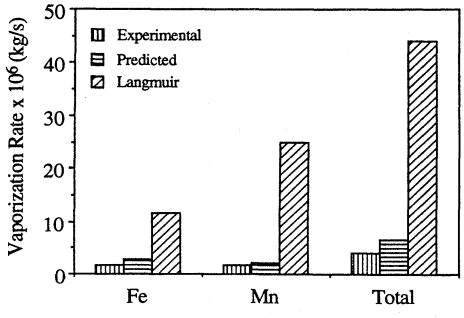

FIG. 11. Comparison of the vaporization rates calculated from the Langmuir equation and from the model with experimentally determined values for AISI 201 stainless steel: laser power, 3000 W; welding speed, 15.24×10^{-3} m/sec; argon flow rate, 5.5×10^{-4} m^3/sec (Mundra and DebRoy, 1993b).

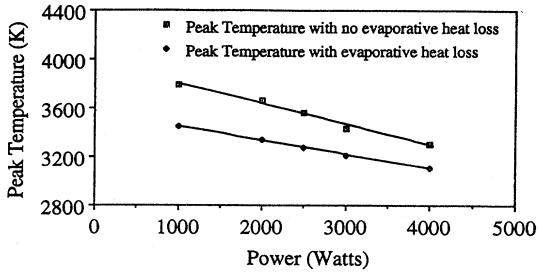

FIG. 12. Effect of evaporative heat loss on peak temperature for different laser powers during welding of AISI 201 stainless steel: welding speed, 15.24×10^{-3} m/sec; argon flow rate, 5.5×10^{-4} m^3/sec (Mundra and DebRoy, 1993b).

where $W(T)$ is the temperature-dependent vaporization flux, L_e is the enthalpy of vaporization, $\Delta\overline{H}$ is the enthalpy of mixing, P is the power density, and x is the fraction of the input power used for vaporization. For various weld-metal compositions and assumed values of x and P, the vaporization rates were estimated from Eq. (15). Based on the relation between the vaporization rate and temperature, given by the Langmuir relation [Eq. (14)], Block-Bolten and Eagar (1982, 1984) estimated weld-pool peak temperatures for various conditions. Their calculations indicated the maximum weld-pool surface temperature to be about 2773 K when Fe-Mn alloys with less than 1% Mn are welded with 6 kW/cm^2 peak input power (Block-Bolten and Eagar, 1982). Based on the values reported in the literature this value is plausible (Kraus, 1989; Choo and Szekely, 1994). Furthermore, they found that when these alloys are welded by laser or electron-beam processes using a peak power density of 10^6 W/cm^2, the peak surface temperature can be in the range 4273–5273 K. These values are higher than the temperatures reported in the literature (Dowden *et al.*, 1985). The peak temperature values estimated from Eq. (15) should be interpreted with caution for the following two reasons. First, the calculation is dependent on the relation between the vaporization flux $W(T)$ and the temperature. As we have discussed in a previous section, reliable calculation of the rates of vaporization of alloying elements from the weld-pool surface requires highly complex numerical calculations involving heat, mass, and momentum balances in both the gas phase and the weld pool. Block-Bolten and Eagar (1982, 1984) used the Langmuir equation to calculate the temperature from the vaporization rate. At one atmosphere pressure, this equation grossly overpredicts the vaporization rate at any given temperature, or for a given vaporization rate, grossly underpredicts the temperature. Since the rate predicted by a straightforward application of the Langmuir equation is up to ten times the actual vaporization rate, much less energy will be lost from the weld pool than predicted by a calculation based on the Langmuir equation. Second, the heat supplied may be used to increase enthalpy and temperature of the pool rather than for evaporation. For example, a weld pool covered by a thin slag layer may be heated to a much higher temperature than the peak temperature calculated from Eq. (15) without losing very much heat owing to vaporization.

When power densities typical of arc welding are utilized, in many cases the heat effect may not be so large as to make a major difference in the temperature field. In contrast, in high-energy-density processes such as laser and electron-beam welding, the evaporative cooling effect is more important. When the thermal effect of evaporation is important, the cooling effect is most pronounced near the middle of the weld pool where the temperature and the vaporization rate are both highest.

E. Metal expulsion due to vapor recoil

Significant vaporization from the weld pool takes place when very high power-density energy sources such as lasers and electron beams are used for welding. In many cases, the escaping vapor exerts a large recoil force, and, as a result, the molten metal is expelled from the cavity. In welding, such metal spatter and weld-metal expulsion are unacceptable, while in drilling, the expulsion of metal from the cavity is desirable. Therefore it is important to know the role of various factors that affect liquid-metal expulsion.

Several investigators have reported experimental results on metal expulsion during laser irradiation. For example, Chun and Rose (1970) irradiated an aluminum target with a Nd-doped glass laser and found that as much as 90% of the material lost was removed from the molten pool as liquid when pulses longer than 200 μsec were used at a power density of 10^7 W/cm^2. However, at low power densities, on the order of 10^5 W/cm^2, melting occurred, but no liquid expulsion took place. Such a condition is favorable for welding. It was discussed in a previous section of this paper that the extent of energy absorption by the workpiece depends on the type of material, the wavelength of the laser, and other factors. Thus it is not possible to prescribe a generally applicable limit of power density to avoid liquid-metal expulsion during welding. Power densities in excess of 10^6 W/cm^2 have been used in welding without liquid expulsion. von Allmen (1976) suggested that the vapor pressure acts like a piston on the liquid weld pool and forces liquid metal out of the cavity. He proposed a model to calculate liquid metal expulsion rate. The convective heat transfer and the conduction heat loss in lateral directions were ignored. Furthermore, the spatial distribution of temperature on the weld-pool surface was not considered for the calculation of the vapor recoil force. The main difficulty in the application of the melt ejection model (von Allmen, 1976) to study the critical conditions for the initiation of liquid-metal expulsion is that the retarding effect of surface tension is not considered. Thus a precondition for the application of the model is that the vapor recoil force must be significantly higher than the surface-tension force. While such a requirement is not unduly restrictive at very high heat-source power densities, it

precludes application of the model to predict conditions for the initiation of liquid-metal expulsion, i.e., when the recoil force just exceeds the surface-tension force.

Basu and DebRoy (1992) examined the conditions for the initiation of liquid-metal expulsion during laser irradiation, experimentally and theoretically. Micrographs of lead and stainless-steel samples irradiated by CO_2 laser pulses are shown in Fig. 13. Melting was observed in each case. However, liquid expulsion did not take place until the pulse length was increased to 0.1 millisecond for lead samples. On varying the frequency and the pulse length for a total exposure time of 1.0 sec, a similar behavior, i.e., the transition from melting to expulsion, was observed in both stainless-steel and titanium samples. A summary of the frequency and pulse-length combinations necessary for initiating liquid-metal expulsion in lead, titanium, and stainless steel is presented in Fig. 14. When irradiated with single pulses, metal expulsion was observed only for large values of pulse length. For multiple pulses, short pulses led to liquid-metal expulsion at higher frequencies when the irradiated region could not cool sufficiently between pulses.

The value of the maximum weld-pool surface temperature just before the initiation of liquid-metal expulsion can be determined from the following criterion. Liquid expulsion takes place when the vapor recoil force overcomes the surface-tension force at the periphery of the

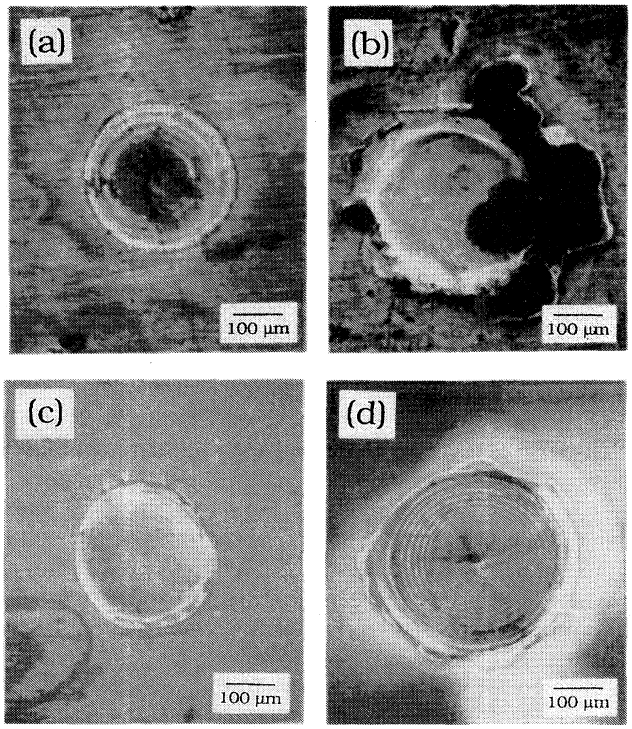

FIG. 13. Micrographs of lead and stainless-steel samples irradiated by laser pulses of increasing duration leading to liquid expulsion. Lead irradiated by single pulses of (a) 0.05 and (b) 0.10 ms durations. Stainless steel irradiated by single pulses of (c) 0.5 and (d) 1.0 ms durations. Laser power, 500 W (Basu and DebRoy, 1992).

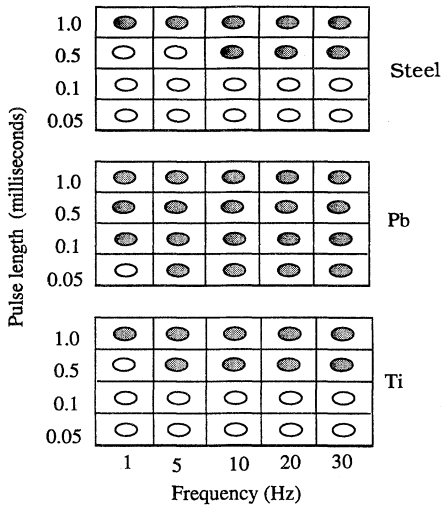

FIG. 14. Combination of pulse length and frequency, which lead to liquid-metal expulsion: cross hatched circles, liquid expulsion; laser power, 500 W (Basu and DebRoy, 1992).

weld pool. For given values of peak temperature T_0, and surface temperature distribution, the recoil force F is calculated (Basu and DebRoy, 1992) from the relation

$$F=2\pi\int_0^{r_b} r\Delta P(r)dr \ , \tag{16}$$

where r_b is the radial distance at which the surface temperature is equal to the boiling point, and $\Delta P(r)$ is the difference between the local equilibrium vapor pressure and the atmospheric pressure and is a function of radial distance from the beam axis. The calculated values of the surface-tension force at the periphery of the weld pool, $2\pi r_0\sigma$, where σ is the surface tension at the melting point, and the recoil force for various values of T_0 are shown in Fig. 15. The details of the calculation procedure and the data used for the calculations are given in a paper by Basu and DebRoy (1992). It is observed that the recoil force is a strong function of the peak temperature. The value of T_0 for which the recoil and surface-tension forces are equal is the critical temperature for liquid expulsion. Liquid expulsion from stainless steel can take place when the temperature at the center of the pool, T_0, exceeds a critical temperature, T_{cr} which is 3380 K. The values of T_{cr}, for lead and titanium are 2120 and 3780 K, respectively (Basu and DebRoy, 1992).

The calculated rise and decay of the peak temperature for stainless steel irradiated by single pulses of length 0.5 and 1.0 millisecond are presented in Fig. 16. It is observed that for a pulse length of 0.5 millisecond, the peak temperature reached is significantly lower than the minimum peak temperature, 3380 K, required for liquid expulsion to occur. However, the peak temperature exceeds the critical temperature for a pulse length of 1.0 millisecond. The results are consistent with the experimental data shown in Fig. 13. Similarly, for lead and titanium, the peak temperature reached in a single pulse could be used to rationalize the experimental observa-

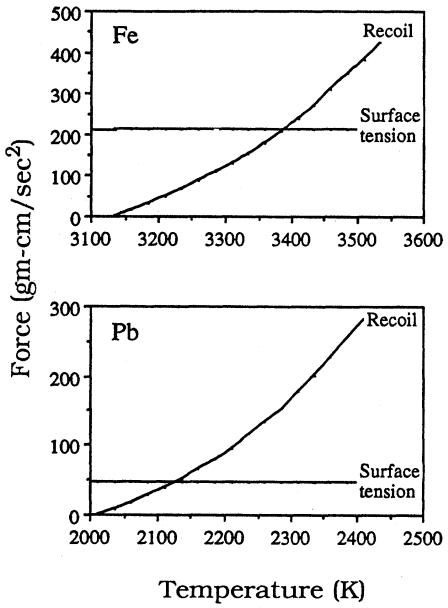

FIG. 15. Recoil force as a function of peak surface temperature and the surface tension force at the melting point for iron and lead (Basu and DebRoy, 1992).

tions. Although there is good agreement between the predicted and the observed condition for metal expulsion, the equations employed are not exact, and the computed temperatures provide dependable trends but are not rigorously computed.

When the peak temperature at the center of the pool exceeds the critical temperature T_{cr}, liquid expulsion takes place. When molten metal is expelled from the weld pool, the laser beam becomes defocused, resulting in a decrease in the heat flux. As a result, the peak temperature may drop below the critical value, and no further expulsion may take place. Thus the extent of melting at the time when the critical temperature is reached determines the amount of liquid-metal expulsion resulting from the vapor recoil effect.

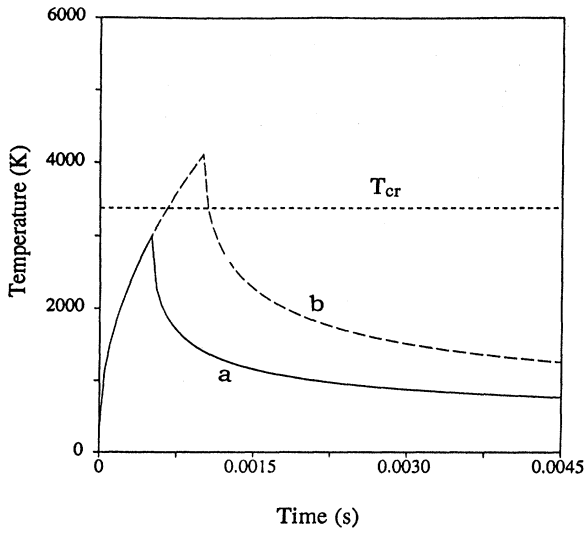

FIG. 16. Peak temperature vs time for a stainless-steel sample irradiated by single pulses of (a) 0.5 and (b) 1.0 ms durations: laser power, 500 W (Basu and DebRoy, 1992).

IV. GAS-WELD METAL REACTIONS

During welding, hydrogen, nitrogen, and oxygen may dissolve in the weld metal, whereupon they subsequently form pinholes or porosity, or combine with elements in the alloy to form inclusions. In steels, hydrogen induces cracking, nitrogen increases the yield strength and the tensile strength but reduces the ductility, and oxygen promotes inclusion formation (Banerjee *et al.*, 1993). Some oxide inclusions can improve toughness by promoting the formation of acicular ferrite in steels.

In arc welding, the consumables can contribute to the weld-metal oxygen and hydrogen concentrations, and slag-metal[3] reactions have a strong influence in determining the concentration of oxygen (Chai and Eagar, 1980; 1981; Indacochea *et al.*, 1985; Mitra and Eagar, 1991a, 1991b, 1991c). In laser welding, the concentrations of hydrogen, nitrogen, and oxygen in the weld metal are affected by the partitioning of these species between the weld pool and the surrounding gas environment.

At the high temperatures reached during welding, reactions of oxygen and nitrogen with the weld metal are rapid, and to avoid extensive dissolution and reaction, some type of shielding is required. This may be achieved by means of flux, gas, or a combination of the two, or from evacuation of the atmosphere, as in electron-beam welding. In electroslag welding, the flux provides shielding of the metal from the atmosphere. In gas-metal arc, gas-tungsten arc and plasma welding, an external gas supply is used. In the welding of reactive metals, special shielding measures such as welding inside a gas filled box are often used to protect the weld metal. In submerged arc welding, depending on the composition of the electrode coating, evolution of CO_2 or other gases such as H_2 can result. The slag helps in protecting the metal. Oxygen and nitrogen contents as high as 0.7 and 0.2 wt. %, respectively, have been obtained in the weld metal during arc welding (Kou, 1987). These concentration levels were far greater than those in the base and filler metals and indicate the importance of dissolution of these species from the gas phase.

A. Dissolution mechanism

In the absence of a slag layer, the dissolution of a species from a diatomic gas environment can be represented as

$$\frac{1}{2}G_2 = \underline{G} \ . \tag{17}$$

[3]Slag is a molten mixture of metal oxides or other inorganic compounds and is immiscible in the weld metal.

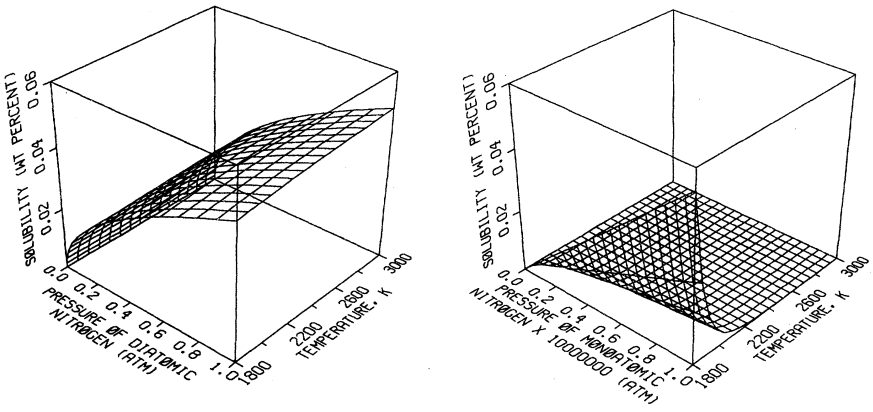

FIG. 17. Computed equilibrium nitrogen concentrations in iron in diatomic and monatomic nitrogen gas environments.

The equilibrium concentration of a species such as hydrogen in a metal is given by Sieverts law, which states that the concentration is proportional to the square root of the partial pressure at any given temperature (Pehlke, 1979).

$$C_{\underline{G}}^{d}=K_{\text{eq}}^{d}\sqrt{p_{G_2}} \tag{18}$$

where $C_{\underline{G}}^{d}$ is the species concentration in solution at equilibrium with the diatomic gas G_2, K_{eq}^{d} is the equilibrium constant for the dissolution reaction (reaction 17), and p_{G_2} is the partial pressure of G_2. However, in most welding processes, the weld metal is exposed to a plasma environment. When a gas transforms to a plasma phase, its constituents may dissociate, ionize, or become electrically or vibrationally excited. All of these species have different equilibria with weld metals. For example, if a plasma contains a significant quantity of some atomic gas, the equilibrium between the atomic gas and the weld metal must be considered. The equilibrium species concentration in a metal in a monatomic gas environment is given by

$$G=\underline{G}\ , \tag{19}$$

$$C_{\underline{G}}^{m}=K_{\text{eq}}^{m}p_G\ , \tag{20}$$

where $C_{\underline{G}}^{m}$ is the species concentration in solution at equilibrium with the monatomic gas G, K_{eq}^{m} is the equilibrium constant for reaction 19, and p_G is the partial pressure of G. Calculation of the equilibrium solubilities from Eqs. (18) and (20) for different gases reveals that, in most cases, the equilibrium concentration of a species in solution is considerably higher in the monatomic gas environment than in the corresponding diatomic gas environment. To illustrate the difference in the equilibrium solubilities, the computed equilibrium concentrations of nitrogen in iron at equilibrium with both diatomic and monatomic nitrogen are shown in Fig. 17. The data used for the calculations are presented in Table I. It is observed that at 1850 K and 1.0 atm of diatomic nitrogen partial pressure, the equilibrium solubility is about 0.045 wt. % $\underline{N}$. However, at the same temperature, in monatomic nitrogen environment, the same equilibrium concentration can be achieved at a partial pressure of only about 1.0×10^{-7} atm. Several investigators (Uda and Ohno, 1973; den Ouden and Griebling, 1990; Gedeon and Eagar, 1990; Bandopadhyay *et al.*, 1992; Banerjee *et al.*, 1993) have concluded that the species concentration in the weld metal can be significantly higher than those calculated from Sieverts law. The transformation of ordinary molecular species to excited neutral atoms and ions

TABLE I. Free-energy/temperature relations used for the calculations. Free-energy data are in cal/gm mole.

Metal/Gas	Reaction	Free-energy/temperature relationship	Reference
Gas phase	$\frac{1}{2}N_2(g)=N(g)$	86596.0−15.659 T	Elliott and Gleiser, 1960
	$\frac{1}{2}O_2(g)=O(g)$	60064−15.735 T	Elliott and Gleiser, 1960
	$\frac{1}{2}H_2(g)=H(g)$	53500.0−14.40 T	Gedeon and Eagar, 1990
Liquid iron/ nitrogen	$\frac{1}{2}N_2(g)=\underline{N}$ (wt. %)	860.0+5.71 T	Pehlke and Elliott, 1963
	$N(g)=\underline{N}$ (wt. %)	−85736.0+21.405 T	
Liquid iron/ hydrogen	$\frac{1}{2}H_2(g)=\underline{H}$ (ppm)	8720.0−11.02 T	Elliott *et al.*, 1963
	$H(g)=\underline{H}$ (ppm)	−44780+3.38 T	Gedeon and Eagar, 1990
Liquid iron/oxygen	$\frac{1}{2}O_2(g)=\underline{O}$ (wt. %)	−28000−0.69 T	Elliott *et al.*, 1963
	$O(g)=\underline{O}$ (wt. %)	−88064+15.045 T	

in the gas phase leads to enhanced solution of species in the metal. The presence of the partially dissociated diatomic gases and electrons in the gas phase introduces several features of the system. Of these, three issues are of special interest in welding. What factors govern the extent of dissociation of a diatomic gas in the welding environment? How does the temperature affect the species concentration in the weld metal for different gases? How many of these dissolved species in the weld pool are still retained by the weld metal after cooling?

The atomic gases in the plasma are formed, in many cases, by a series of reactions involving inelastic collisions of the diatomic molecules with electrons (Bandopadhyay *et al.*, 1992). The properties of the plasma such as the electron density and energy affect the formation of various atomic, ionic, and excited neutral species from the diatomic molecules. Determination of the nature and the concentration of various species within the plasma is the key to a quantitative understanding of the enhanced solution of nitrogen, oxygen, and hydrogen in the weld metal.

Bandopadhyay *et al.* (1992) studied the plasma-enhanced nitrogen solubility in pure tantalum and niobium at 2243 K. Samples of these metals were equilibrated under helium-nitrogen mixtures. The results of their study with tantalum are presented in Fig. 18. The plot shows a much greater nitrogen solubility in the presence of a plasma than without for the same level of diatomic nitrogen in the source gas. From the optical emission spectra of the plasma, they determined that the plasma contained nitrogen molecules and atoms in both neutral and ionized states. The enhanced solubility was attributed to the presence of atomic nitrogen in the plasma. Work is now underway at Penn State and elsewhere to relate the properties of the plasma with the concentrations of various species in the plasma.

The effect of temperature on the equilibrium concentrations of hydrogen, nitrogen, and oxygen in iron in pure diatomic and monatomic gas environments is presented in Figs. 19 and 20, respectively. The equilibrium species concentrations increase slightly with increasing temperature for nitrogen and hydrogen. However, for molecular oxygen, the equilibrium concentration decreases with increasing temperature. In the case of the three pure monatomic gases, the equilibrium concentrations decrease with increasing temperature (Fig. 20). In other words, for a given partial pressure of atomic gas, the equilibrium concentration of a solute increases with decreasing temperature. Thus, if equilibrium were to be achieved, the concentrations of these solutes would be much higher near the periphery of the weld pool than at the middle, where the temperature is commonly much higher than that of the melting point of the alloy. However, the attainment of equilibrium under welding conditions may not be practical for various reasons. First, since the concentrations of the atomic species in the gas phase are very small, and since the atomic species are mixed with the molecular species in the gas phase, the probability of collision of the atomic gases with the free surface of the metal is low. Most of the surface sites will collide with the diatomic molecules in preference to the monatomic gases. However, all collisions do not lead to absorption. The probability of a collision leading to absorption is determined from the sticking probability. Second, the duration of exposure of a particular monitoring location to very high temperatures is short. Therefore the potentially rapid dissolution rate may not insure attainment of equilibrium. The quantitative prediction of partitioning of these elements between the weld pool and its surroundings remains a problem of major importance.

After the elements are dissolved in the weld pool, their

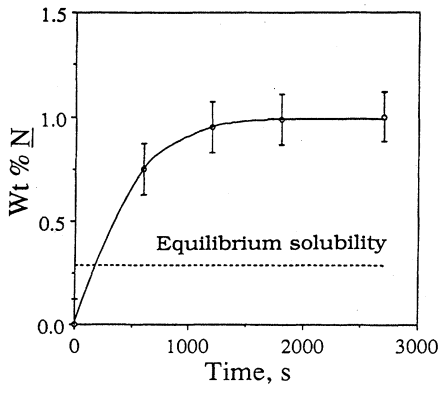

FIG. 18. Weight percent nitrogen versus time for dissolution of nitrogen in tantalum at 2243 K: partial pressure of nitrogen in the plasma source gas, 1.12 Pa (Bandopadhyay *et al.*, 1992).

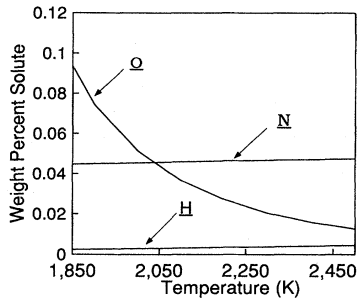

FIG. 19. Effect of temperature on the equilibrium concentration of hydrogen, nitrogen, and oxygen in iron in diatomic pure gas environments ($p_{N_2}=1$ atm, $p_{O_2}=10^{-9}$ atm, $p_{H_2}=1$ atm.)

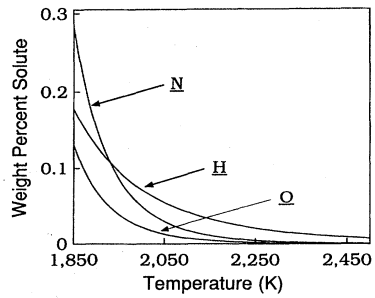

FIG. 20. Effect of temperature on the equilibrium concentration of hydrogen, nitrogen, and oxygen in iron in monatomic pure gas environments ($p_N=10^{-6}$ atm, $p_O=10^{-8}$ atm, $p_H=5\times10^{-2}$ atm).

concentrations change with time during solidification and cooling. Gedeon and Eagar (1990), in their study of hydrogen dissolution, observed that a model for hydrogen dissolution in the weld metal must take into account the mechanism of hydrogen absorption in the weld pool, hydrogen rejection from the solidifying front, and the hydrogen diffusion away from the weld pool. Since the diffusivity of hydrogen is much higher than that of nitrogen or oxygen, the rate of diffusion of nitrogen or oxygen away from the weld pool is likely to be lower than that of hydrogen. A fundamental understanding of the rates of dissolution of hydrogen, oxygen, and nitrogen in the weld pool, and their rejection from and transport in the liquid and the solid phases during solidification and cooling is just beginning. Because of the important role of these species in determining the properties of weld metal, understanding their origin and science-based control remains an important goal in welding research.

B. Inclusions

In steel weldments, oxide, nitride, and sulfide inclusions may be present, and among these, the oxide inclusions are most common. In general, the presence of inclusions is detrimental to weld properties. However, under a given set of conditions, in low alloy steel welds, certain oxide inclusions are known to promote the formation of an acicular ferrite phase, which, in turn, improves toughness. On the other hand, the presence of a very high volume fraction of inclusions, though, may initiate premature ductile fracture.

Although the importance of inclusions in affecting weld-metal properties has been recognized for a long time, it is only in recent years that systematic studies of inclusions in weld metals have started. Frost *et al.* (1993) showed that microsegregation during weld-pool solidification can cause significant increases in the concentrations of oxygen and deoxidants in the interdendritic liquid. They used the available equilibrium data for oxide dissolution to predict the sequence of precipitation for various oxides during the solidification process. Kluken and Grong (1989) determined the volume fraction of inclusions from an empirical relation involving both oxygen and sulfur concentrations. They modeled the size and chemical composition of inclusions in the low-alloy steel weld from the knowledge of weld-metal chemistry and the welding conditions.

The rate of precipitation of the oxide inclusions from a supersaturated solution can be determined from the rate of diffusion of the elements to the reaction interface. The diffusion rate coupled with the nucleation rate can provide the growth kinetics of the various types of inclusions. A comparison of the transformation time for various oxides as a function of temperature, based on the calculations of Babu *et al.* (1994), is shown in Fig. 21. For the composition of the weld metal, the first oxide to form is Al_2O_3. As the weld cools further, the sequence of inclusion formation in terms of composition is

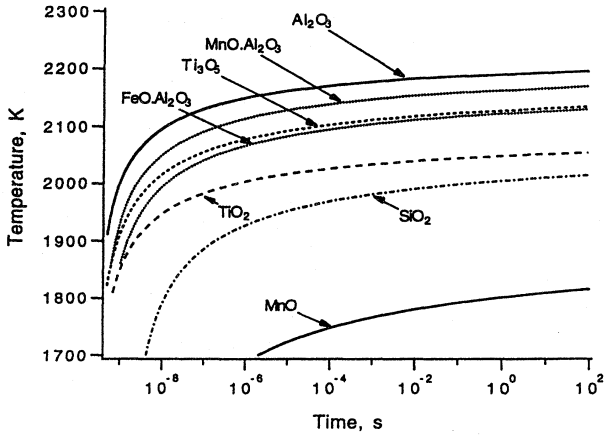

FIG. 21. A comparison of the formation time for 10% of final amount for various oxides as a function of time. Calculations are done for a weld-metal composition of 0.066% C, 0.82% Si, 1.66% Mn, 0.025% Ti, 0.026% Al, and 0.086% O. The sequence of oxide formation during weld cooling can be predicted as described in the text (Babu *et al.*, 1994).

$MnO{\cdot}Al_2O_3$, Ti_3O_5, $FeO{\cdot}Al_2O_3$, TiO_2, SiO_2, and MnO. Diagrams of these types can be used to predict the sequence of oxidation reactions as a function of temperature and composition. Babu *et al.* (1994) have shown that an estimate of the observed number density of inclusions in the weld metal can be made from the cooling rate and the nucleation rate of the first forming oxide.

Although significant progress has been made in recent years in understanding the formation and behavior of inclusions, several important issues remain to be addressed. For example, the exact mechanism for the changes in the inclusion characteristics with the welding parameters, such as heat input, is not well understood. A comprehensive understanding of the inclusion volume fraction, size, number density, and composition for well-defined welding conditions still remains to be developed.

V. DEVELOPMENT OF WELDMENT STRUCTURE AND PROPERTIES

The process-microstructure-property relationships are important for the understanding of the structure, properties, and performance of the welded materials. Unfortunately, many of the basic principles relating to these relationships are not well understood, mainly because of the complexities inherent in fusion welding, such as unknown weld-pool shape, formation of nonequilibrium microstructures, and spatial variations of composition, microstructure, and properties. Extensive local variations of composition and microstructures in a weldment are common and unique to welded structures. In addition, due to localized heating during welding, complex thermal and transformation stresses are generated that remain in the weldment as residual stresses.

The origin of microstructural and stress gradients and

their influence on the weld performance is a largely unexplored field, in part, due to the lack of understanding of the formation of these gradients. Furthermore, the characterization tools to probe these gradients on both macroscopic and microscopic scales have been developed fairly recently. Recent advances in the techniques for the determination of microstructures and mechanical properties are ideally suited for examination of welds with microstructural and composition gradients (David, Goodwin, and Braski, 1979; Vitek and David, 1990).

Developments in microstructural characterization techniques, such as analytical electron microscopy, scanning electron microscopy, and atom probe field ion microscopy, have made it possible to characterize microstructures on scales as fine as a few nanometers. To clarify experimental data obtained under welding conditions, simulation techniques, such as differential thermal analysis, thermomechanical simulation, and welding of single crystals, have been successfully used to understand microstructural development (Vitek and David, 1990; Cieslak, 1991). Because of the spatial variation of weld properties, fine-scale evaluation of properties is often desirable. Recent techniques such as nanoindentation hardness testing, indentation creep testing, and miniature impact specimen testing (Vitek and David, 1990) have made it possible to evaluate welds by performing tests on small areas, often with the use of miniature test specimens. Neutron scattering analysis can characterize stresses in materials on a millimeter scale. Thermal neutrons, which can penetrate 50 mm into steel, have recently been used (Root *et al.*, 1993a, 1993b) to characterize residual stresses in weldments (Fig. 22). Measurement of the stress magnitudes and distribution is crucial to understanding alterations of phase transformation behavior in a welding environment and to predicting fracture behavior in welds. Use of these advanced experimental and analytical techniques is enabling us to better characterize and understand weld microstructures, properties, and stresses.

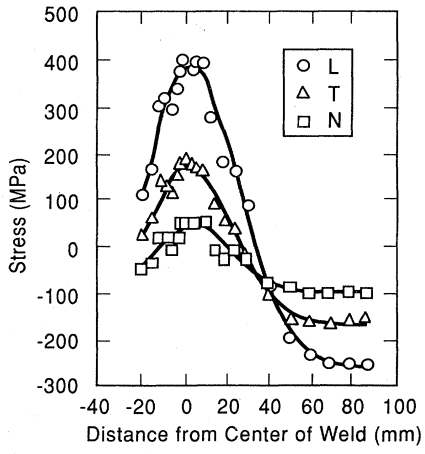

FIG. 22. The averaged stresses [longitudinal (L), transverse (T), and normal (N)] in the welded plate (Courtesy of S. Spooner, Oak Ridge National Laboratory).

Currently, efforts are under way to study the fusion zone and the heat-affected zone characteristics and, in particular, the solidification behavior of the weld-pool and the solid-state transformations in weldments. Over the years, significant work has been done on the mechanical behavior of weldments. However, a critical issue that remains is the fracture behavior of weldments, as influenced by microstructural and stress gradients. To date, the development of the theory and application of fracture mechanics has been directed toward homogeneous materials such as the base metal, with little consideration of the special problems that the inhomogeneous structures of the weldment might impose. Therefore significant opportunities exist to develop the theory and methodologies for treating fracture mechanics in the presence of both microstructure and stress gradients.

A. Weld-pool solidification

1. Basic parameters

During welding, as the weld pool undergoes transformation from liquid to solid, the solidification behavior controls solute redistribution, solidification structure, the size and shape of grains, and the distribution of inclusions and defects, such as porosity and hot cracking. Most of our current knowledge of the weld-pool solidification is derived from an extrapolation of the knowledge of freezing of castings, ingots, and single crystals at lower thermal gradients and growth rates (David and Vitek, 1989). Parameters critical in determining the fusion zone microstructures are growth rate R_S, temperature gradient G, undercooling ΔT, and alloy constitution. The temperature gradient and growth rate are important in the combined forms G/R_S and GR_S (cooling rate) as they influence the solidification morphology and the scale of the solidification substructure, respectively. In welding, where the molten pool is translated through the material, both G and GR_S vary considerably across the fusion zone. Depending on the type of welding process and the location, the maximum cooling rate GR_S encountered within the weld pool may range from 10^2 to 10^7 °C/sec.

Temperature gradients in the solid G_S and in the liquid G_L at the solid/liquid interface play a significant role in determining the solidification substructure in the fusion zone. The thermal gradient in the liquid is more critical in determining the morphology of the solid/liquid interface. Evaluation of G_L is complicated by the fact that it is strongly influenced by convection in the weld pool. Although it is difficult to determine these parameters accurately, attempts have been made to measure them experimentally (Nippes *et al.*, 1955; Nippes *et al.*, 1957; Matsuda *et al.*, 1969; Garland, 1972). Computational modeling can provide a reasonable alternative to experimental measurements by allowing thermal gradients in the weld pool to be calculated.

Growth rate or solidification rate is the rate at which

the solid/liquid interface in the weld pool advances. The growth rate varies considerably with location in the weld pool. During steady-state welding, the rate at which the solid/liquid interface advances can be related to the rate and direction of the moving heat source if one knows the weld-pool shape (Davies and Garland, 1975; Savage, 1980; Rappaz, Carrupt, *et al.*, 1987; Rappaz, Gremaud, *et al.*, 1987). Since the direction in which the solidification front moves is along the maximum thermal gradient, which is also normal to the solid/liquid interface, the solidification rate $\mathbf{R}_S$ is related to heat-source velocity $\mathbf{R}_H$ by (Rappaz, Carrupt, *et al.*, 1987)

$$|\mathbf{R}_S| = \mathbf{R}_H \cdot \mathbf{n} = |\mathbf{R}_H| \cos\theta \ , \tag{21}$$

where $\mathbf{n}$ is the unit direction normal to the solidification front, parallel to $\mathbf{R}_S$, and θ is the angle between the surface normal $\mathbf{n}$ and the welding direction. However, this does not take into account the influence of growth crystallography. In metals and alloys, there are specific preferred growth directions known as "easy growth" directions (Flemings, 1974). For cubic metals, the easy growth directions are $\langle 100 \rangle$. For dendritic growth along a general crystallographic direction $[hkl]$, the dendritic growth rate $\mathbf{R}_{hkl}$ is related to the solidification rate $\mathbf{R}_S$ by

$$|\mathbf{R}_S| = \mathbf{R}_{hkl} \cdot \mathbf{n} = |\mathbf{R}_{hkl}| \cos\psi \ , \tag{22}$$

where ψ is the angle between the solidification front normal and $[hkl]$. Therefore the dendritic growth rate is given by

$$|\mathbf{R}_{hkl}| = |\mathbf{R}_H| \frac{\cos\theta}{\cos\psi} \ . \tag{23}$$

These relationships are illustrated in Fig. 23.

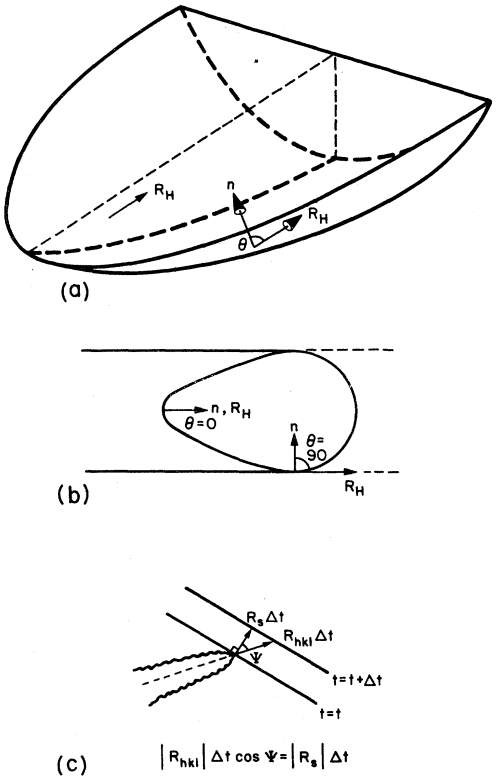

FIG. 23. Schematic diagram illustrating relationships between heat-source velocity (R_H) and solidification front growth rate (R_S): (a) Identifies vector quantities; (b) top view of weld pool; (c) incremental change in surface position during time Δt of small section element of surface (David and Vitek, 1989).

Undercooling is a critical parameter that controls the solidification microstructure and segregation effects. The term undercooling, ΔT, means how far a liquid alloy of given composition is cooled below its equilibrium liquidus temperature. Undercooling may be associated with the nucleation of a solid in the liquid or with the growth process during solidification. Unlike in castings, weld solidification proceeds from the preexisting solid substrate, and, hence there is little or no nucleation barrier. Therefore, for welds, the only undercooling of importance is the growth undercooling associated with weld solidification. The total undercooling for growth, ΔT, is comprised of contributions from thermal, ΔT_{TH}, constitutional, ΔT_C, kinetic, ΔT_K, and solid curvature, ΔT_R, effects:

$$\Delta T = \Delta T_{\mathrm{TH}} + \Delta T_C + \Delta T_K + \Delta T_R \ . \tag{24}$$

For most welding conditions in metals and alloys, thermal undercooling, ΔT_{TH}, and the kinetic undercooling, ΔT_K, are minimal and can be ignored. Therefore, for a growing solid in the weld pool, only the constitutional undercooling, ΔT_C, and undercooling due to curvature effects, ΔT_R, are important. In welds, since the microstructures are much finer in scale than in castings, the contribution to the total undercooling due to the curvature, ΔT_R, that is, the dendrite tip undercooling will be very significant. The total undercooling has a significant influence on the solidification morphology and the extent of microsegregation of elements during weld solidification. The effect of increased undercooling at the dendrite tips is to solidify at a composition closer to the overall alloy composition and thus reduce microsegregation.

2. Nucleation

The development of the fusion zone microstructures can be interpreted by considering classical ideas of nucleation theory as well as growth behavior. In conventional solidification, nucleation may be discussed under two separate categories, namely, homogeneous and heterogeneous nucleation. When solid forms from the liquid without the aid of foreign material, it is said to nucleate homogeneously. Such a process requires a large

driving force or an equivalently large undercooling below the freezing point. The free energy of formation of a critical-sized nucleus of solid, ΔG^*, is given by

$$\Delta G^* = \frac{16\pi\gamma_{SL}^3}{3\Delta G_v^2} , \tag{25}$$

where γ_{SL} is the solid/liquid interfacial energy and ΔG_v is the free-energy change-per-unit volume for solidification. However, if the melt contains foreign solid matter such as oxides or other solid particles, nucleation of the solid may be facilitated. In such a case, the free energy of formation of a critical-sized nucleus, ΔG^*_{het}, is less than ΔG^* by the factor $f(\beta)$:

$$\Delta G^*_{het} = \Delta G^* f(\beta) , \tag{26}$$

where $f(\beta)$ is a shape factor that depends on the wetting angle. For heterogeneous nucleation, $f(\beta) \ll 1$, indicating a significantly decreased nucleation barrier.

In welds, since solidification proceeds from the preexisting solid substrate, $f(\beta)$ approaches zero. Thus the nucleation barrier becomes very small and solidification occurs spontaneously by epitaxial growth. In addition, the more classical case of heterogeneous nucleation may also apply if nucleation barriers are sufficiently reduced. Inoculants can be used to promote nucleation in welds. Finally, dynamic methods such as pool stirring and arc oscillations may be used to fragment and dislodge dendrites from the solidification front so that they can act as nuclei for the growth of additional grains. However, an understanding of the principles of refinement in fusion-zone grain structure, using all of these techniques, needs to be developed. Fluid flow computational models need to be coupled with microstructural development to ascertain the influence of convective flow on dendrite fragmentation and the refinement of the fusion-zone grain structure.

3. Growth

In the presence of a preexisting solid/liquid interface in the fusion zone, growth of the solid occurs by the addition of atoms from the liquid to the solid. The ease with which this can happen, or the kinetics of growth, is controlled to a large extent by the interface structure on an atomic scale. The growth of the solid can occur by two-dimensional growth, by growth on a screw dislocation, or by uniform or continuous growth (Flemings, 1974; Biloni, 1987). The stability of the interface is critical in determining the microstructural characteristics of the weld metal. During the growth of the solid, the microscopic shape of the solid/liquid interface is determined by the thermal and constitutional conditions in the immediate vicinity of the interface. These factors determine whether growth occurs by planar, cellular, or dendritic mode (Fig. 24). Theories for interface stability under conditions of equilibrium at the interface for normal solidification, or under extreme nonequilibrium conditions prevalent during rapid solidification, have been developed (Flemings, 1974; Kurz and Fisher, 1986). Further, in recent years significant advances have been made in the theory and fundamentals of dendritic solidification (Glicksman, 1989; Langer, 1989). These theories can be applied to advance our understanding of weld-pool solidification.

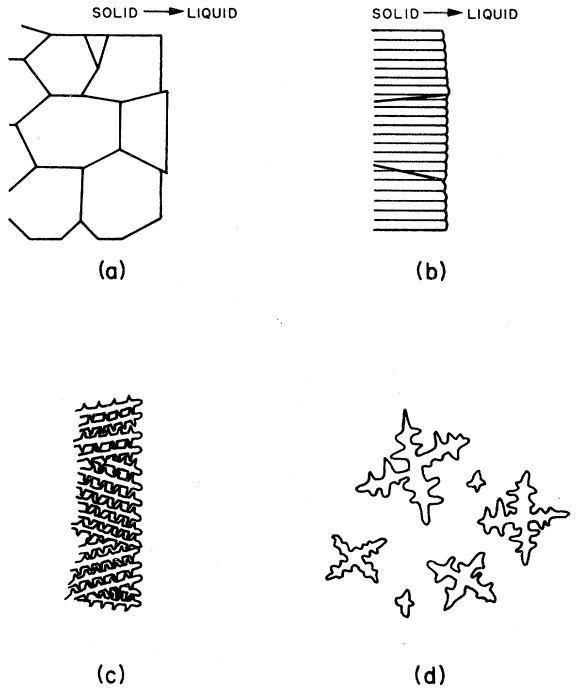

FIG. 24. Various structural morphologies possible during solidification: (a) plane front growth; (b) cellular growth; (c) columnar dendritic growth; (d) equiaxed dendritic growth (David and Vitek, 1989).

In pure metals, without any solute effects, only thermal gradients control the stability of the solid/liquid interface. In alloys, the solidification front stability is more complex. Since there is a partitioning of solute elements between the solid and liquid during solidification, composition gradient effects ahead of the interface must be considered. The effect of solute redistribution and buildup of solute at the solid/liquid interface on the morphological stability of the solidification front has been examined by considering the concept of constitutional supercooling (Flemings, 1974; Kurz and Fisher, 1986). The criterion for constitutional supercooling for plane front instability can be written as

$$G_L/R_S < \Delta T_0/D_L , \tag{27}$$

where G_L and R_S are as defined earlier, ΔT_0 is the equilibrium solidification temperature range at a given composition, and D_L is the solute diffusion coefficient in liquid. If $G_L/R_S > \Delta T_0/D_L$, the plane front will be stable.

The constitutional supercooling criterion for plane front stability is shown graphically in Fig. 25. For

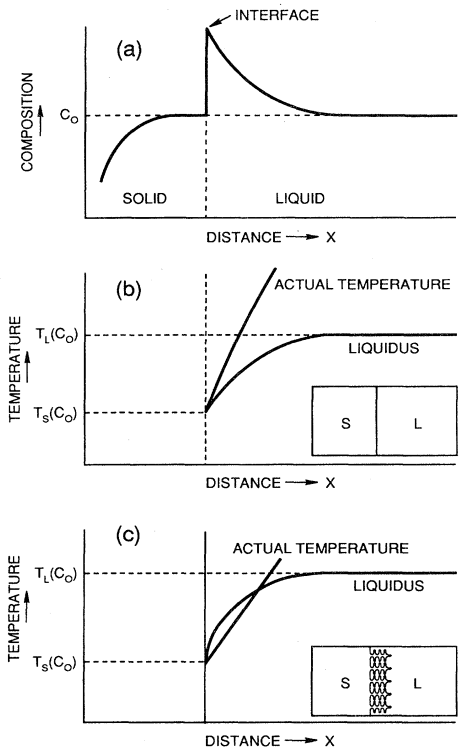

FIG. 25. Development of constitutional supercooling during plane front alloy solidification: (a) composition profile and solute enrichment layer ahead of steady-state planar solidification front; (b) condition for plane front stability; (c) condition for unstable plane front and constitutional supercooling.

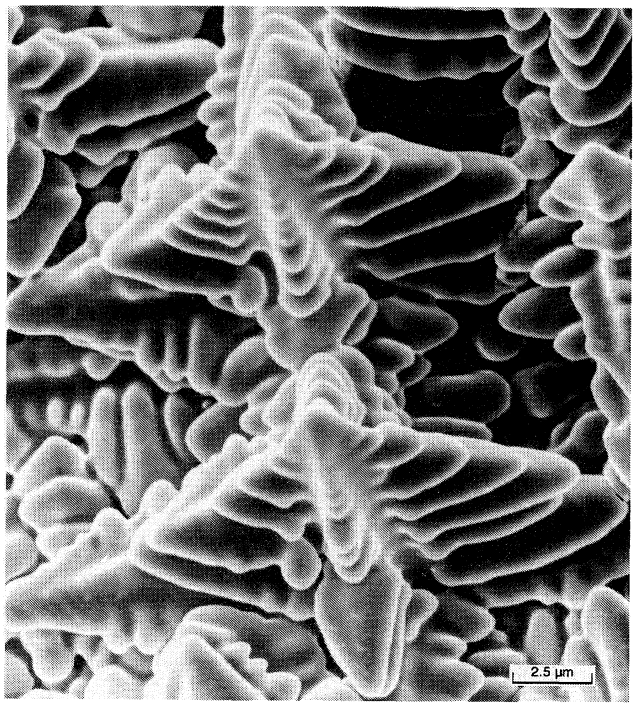

FIG. 26. Scanning electron micrograph showing the development of dendrites in a nickels-based superalloy single-crystal electron beam weld. The primary, secondary, and tertiary dendritic arms are clearly discernible (David and DebRoy, 1992).

steady-state plane front growth, the solute composition profile is as shown in Fig. 25(a). The corresponding temperature profile for the equilibrium liquidus temperature is shown in Figs. 25(b) and 25(c). Depending on the actual thermal gradient in the liquid, the plane front will remain stable [Fig. 25(b)] or it will become unstable [Fig. 25(c)]. As the growth conditions depart from planar stability, the interface morphology will change from planar to cellular to dendritic. If the conditions are favorable, the dendrites will exhibit secondary and tertiary arms in crystallographically predetermined preferred growth directions. Figure 26 shows dendritic growth of the solid, with its multiple branches, observed during welding of a single-crystal nickel-base superalloy.

The concept of constitutional supercooling is very useful for broadly understanding the development of microstructure and the influence of process parameters on weld microstructures, but it is not sufficient to describe precisely, and in quantitative detail, the morphological stability at the solidification front. More rigorous analyses by Mullins and Sekerka (1964) and others (Trivedi, 1970; Kurz and Fisher, 1981; Kurz *et al.*, 1986; Trivedi and Kurz, 1986) have been developed to evaluate additional conditions for plane front solidification. The input data necessary for the application of the solidification models, such as the cooling rate, are difficult to prescribe accurately. Meaningful application of these models to welding remains an important goal for advancing our understanding of the structure of the welded materials.

4. Solute redistribution

It is well established that extensive solute redistribution occurs during solidification of alloys. Solute redistribution is an important phenomenon in welding, resulting in the segregation of elements that can significantly affect weld cracking, microstructure, and properties. In particular, segregation of low melting temperature constituents such as sulphur and phosphorus into the liquid during weld-pool solidification may induce cracking of the weld. Segregation on a fine scale with dendrite arm spacings in the range of 10 to 100 μm is called microsegregation. When the scale is as large as several hundreds of micrometers, the segregation is known as macrosegregation. A limited amount of theoretical and experimental work has been done to describe the solute redistribution during weld-pool solidification. These studies are extensions of different models proposed to describe the solute redistribution that occurs during solidification of castings and single crystals.

The compositional effects of solidification of alloys can be divided into three cases (Flemings, 1974; Biloni, 1987). These situations are also important in understanding weld-pool solidification. Case I is the equilibrium

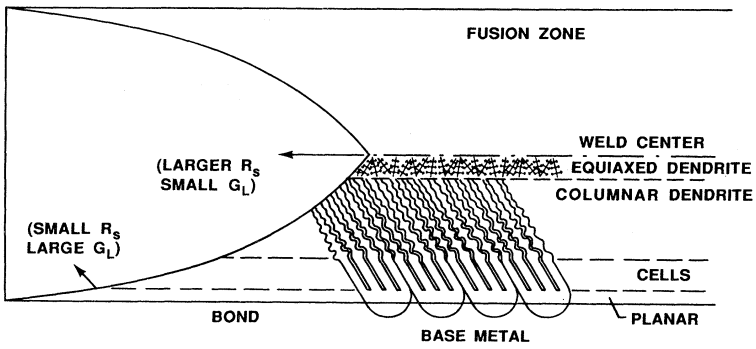

FIG. 27. Schematic diagram of structural variation of weld microstructure across the fusion zone (David and Vitek, 1989).

solidification with complete solid and liquid diffusion of the solute. This case does not generally apply to welding situations. Case II assumes little or no diffusion in the solid, while complete mixing in the liquid by convection and diffusion is presumed. This condition leads to microsegregation effects in weld microstructures. Case III assumes no diffusion in the solid and limited diffusion in the liquid, with no convection. This case allows for the buildup of a solute boundary layer ahead of the solid/liquid interface. Case III is used to describe morphological stability and microstructural development in welds as described in Sec. V.A.3.

In a weld microstructure, generally three types of microstructures can be recognized (Fig. 27). Often, a plane front solidification structure is found along the fusion line, a columnar dendritic structure exists in the interior of the weld, and sometimes an equiaxed region is present in the center of the weld. For the region of the weld that shows plane front solidification, case III solidification, defined earlier, with limited diffusion in the liquid, is most appropriate to analyze solute redistribution.

When describing solute redistribution under dendritic growth conditions for welds, consideration should be given to redistribution both at the dendrite tip and in the interdendritic regions. The solute redistribution at the dendrite tip is determined, to a large extent, by the dendrite tip undercooling, as described earlier. Dendrite tip undercoolings in welds have been estimated by measuring dendrite core compositions in two different alloy systems, Al-Cu and Fe-Nb, after GTAW welding (Brooks and Baskes, 1986). The estimated dendrite tip undercoolings have been found to be significant. Considering the solute redistribution in the interdendritic regions, it may be sufficient to extend the solidification model (case II) for microsegregation in castings to welds. In the analysis, lateral growth of dendrites is approximated by considering planar solidification in a small volume element, as shown in Fig. 28. It is also assumed that no diffusion occurs in or out of this volume element. In this case, the composition of the solid is given by the Scheil equation (Scheil, 1942):

$$C_s^* = kC_0(1-f_s)^{k-1} , \tag{28}$$

where C_s^* is the solid composition, f_s is the volume fraction solid, C_0 is the overall alloy composition, and k is the equilibrium partition coefficient. This equation was modified by Brody and Flemings (1966) by allowing for diffusion in the solid during solidification. Kurz and Clyne (1981) have further refined Brody and Fleming's model to account for extensive solid diffusion. These models can be adapted to analyze microsegregation in welds. Brooks and Baskes (1986) have calculated and measured microsegregation in Al-Cu and Fe-Nb welds. Extension of these models to welds in ternary and higher-order alloy systems remains a challenge. Furthermore, a basic understanding of weld cracking phenomena based on segregation behavior in complex alloys and weld processing parameters is necessary in solving major weldability problems (Patterson and Mahin, 1990; Lin *et al.*, 1993).

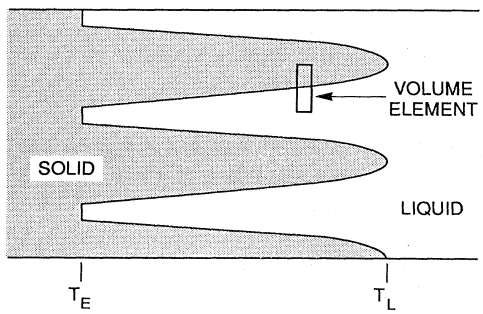

FIG. 28. Volume element used in calculating microsegregation across dendrites (David and Vitek, 1989).

5. Grain structure

The weld-metal or fusion-zone grain structure is predominantly controlled by the base-metal grain structure and the welding conditions. Initial growth occurs epitaxially at the partially melted grains in the base metal (Davies and Garland, 1975; Savage, 1980; David and Liu, 1982). In polycrystalline weld specimens, among the randomly oriented grains in the base metal, those grains whose ⟨100⟩ directions are most closely aligned with the heat flow direction will be favored. The preferred grain selection process that occurs during welding promotes a columnar structure (Kerr and Villafuerte, 1992), as shown in Fig. 29.

Our current understanding of the development of fusion-zone grain structure in polycrystalline welds is

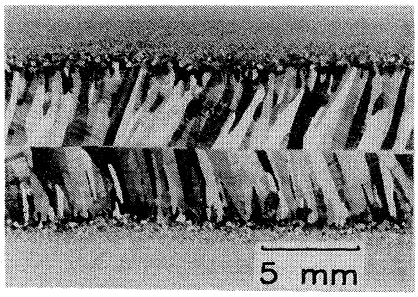

FIG. 29. Columnar grain structure in a steel weld (Courtesy of H. W. Kerr, University of Waterloo, Waterloo, Canada).

limited because the details of the growth selection process and the three-dimensional (3D) pool shape are obscured by the multitude of grains and grain orientations present in polycrystalline materials. However, progress has been made in understanding the fusion microstructure development in single-crystal welds. Recent work (Rappaz *et al.*, 1989, 1990; David *et al.*, 1990) has examined the effect of growth crystallography and the dendrite selection process on the development of the fusion-zone microstructures in single crystals. In these investigations, the goal was to predict the stable dendrite growth direction as a function of pool shape for various crystal orientations. From the observed dendritic arrangements, a 3D reconstruction of the weld pool is possible, as shown in Fig. 30. This analysis has been extended to evaluate the competitive dendritic growth behavior in bicrystal welds (Vitek *et al.*, 1993). Future work to extend these studies to polycrystalline welds is important.

6. Rapid solidification effects

In analyzing weld-pool solidification characteristics, one of the basic assumptions in extending conventional

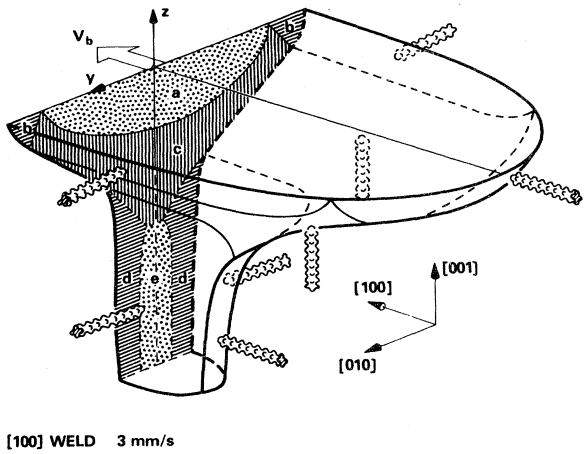

FIG. 30. Three-dimensional schematic diagram of a weld pool. The weld-pool shape was constructed using several two-dimensional transverse optical micrographs of Fe-15Ni-15Cr alloy single crystal welds (Rappaz *et al.*, 1989).

solidification theories to weld-pool solidification is that equilibrium is maintained at the solid/liquid interface. This may be true for welds that are made using conventional welding processes, such as gas-tungsten arc, submerged arc, and electroslag welding processes, in which the cooling rates encountered may range from 10^2 to 10^3 °C/sec. However, this assumption is not valid at rapid cooling rates experienced by the weld pool during high-energy density processes such as laser and electron-beam welding. In recent years, these processes are gaining more attention. In order to understand the development of the microstructures under these conditions, reference must be made to literature on rapid solidification (Duwez *et al.*, 1960; Mehrabian, 1982; Steeb and Warlimont, 1985; Kurz and Fisher, 1986; Kurz and Trivedi, 1989).

As a result of rapid solidification encountered during welding, a wide range of effects may result. These include drastic changes in the partition coefficient k, formation of nonequilibrium phases, and changes in the general microstructural features, mostly in scale. During solidification under equilibrium conditions at the solid/liquid interface, the equilibrium partition coefficient k, may be obtained from the tie lines in the phase diagram. However, at rapid cooling rates, the solid/liquid compositions at the interface are not in equilibrium. This effect is accounted for with the use of nonequilibrium partition coefficient, k'. Several models have been developed to evaluate for k' and determine its variation with solidification velocity (Baker, 1970; Aziz, 1982; Wood, 1982; Cahn *et al.*, 1979; Jackson *et al.*, 1979; Boettinger and Coriell, 1984). Some of the consequences of nonequilibrium solidification at high-solidification rates are less solute partitioning (and, hence, less segregation) and an extension of the solid solubility limit. Finally, it should be pointed out that rapid cooling rate effects also drastically influence the scale of the solidification substructure, namely, cell spacing or primary and secondary dendrite arm spacings.

Another effect of rapid solidification conditions in welds that has received a great deal of attention in recent years is the formation of nonequilibrium phases (David and Vitek, 1982; Vitek *et al.*, 1983; Katayama and Matsunawa, 1985, 1986; David *et al.*, 1987; Venkataraman and Devletian, 1988; Elmer *et al.*, 1989; Brooks *et al.*, 1991; Lippold, 1994). These studies have shown that nonequilibrium solidification may occur in a wide range of stainless-steel alloy compositions. Figure 31 shows a fully austenitic stainless-steel weld microstructure in a laser weld, which would normally contain a duplex austenite and ferrite microstructure. The origin of this microstructure has been attributed to a change in the mode of freezing. For example, at the large undercoolings encountered at rapid cooling rates, the stainless-steel liquid solidifies as austenite and not as ferrite. The various factors that control this nonequilibrium effect and the extent to which nonequilibrium phases form in welds cooled under rapid solidification conditions are not yet fully understood. Future efforts in this area should in-

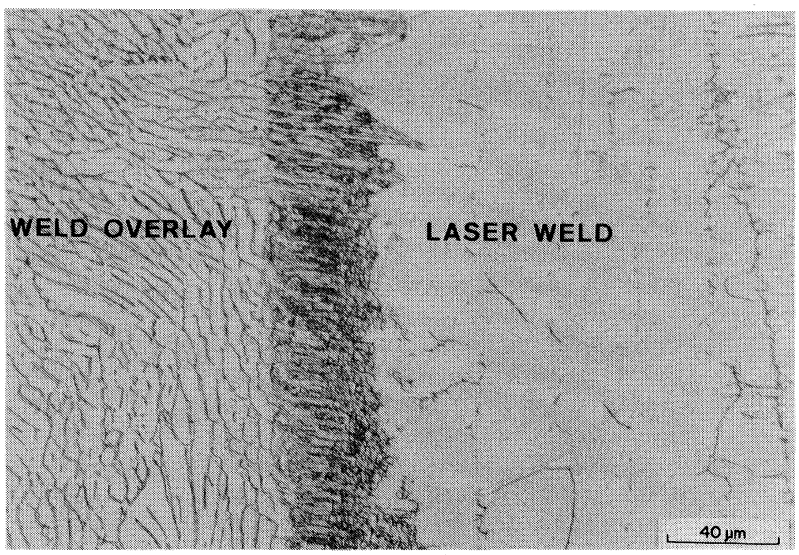

FIG. 31. Duplex (austenite and ferrite) structure modified by laser welding to produce a fully austenite structure (David and Vitek, 1982).

volve both theory and experimentation to understand this phenomenon and its implication on the cracking sensitivity of nonequilibrium microstructures produced under rapid cooling conditions.

B. Solid-state transformations

During welding, extensive solid-state phase transformations occur both in the fusion zone and the heat-affected zone (Easterling, 1992). They may occur during welding of single-phase or polyphase metals. In the fusion zone, the solid-state transformations occur during postsolidification cooling to ambient temperature. In the heat-affected zone, the transformations occur during both the heating and cooling segments of the thermal cycle. The extent of these transformations varies across the weldment and is a function of both the heating and cooling rates and the maximum temperatures attained during the thermal cycle. Depending on the severity of the thermal cycle and the magnitude of the temperature gradient, the heat-affected zone can often be conveniently divided into several subzones. Each of these zones will exhibit different phase-transformation characteristics. As a result, the heat-affected zone often exhibits compositional, microstructural, and property gradients. It is not an exaggeration to suggest that all of the phase changes known in metallurgy can be found in either the fusion-zone or the heat-affected zone of a typical weldment. These include solidification, chemical segregation, solid-state phase transformations, recrystallization, recovery, grain growth, precipitation, coarsening, and stress-affected transformations. Furthermore, most of these processes occur at rates that are far from equilibrium and certainly under nonisothermal conditions. Therefore a thorough evaluation of phase transformations and microstructural development during welding requires consideration of both heating and cooling behaviors. To date, nearly all phase-transformation studies in the literature emphasize development of microstructures under controlled isothermal annealing or continuous cooling conditions. However, phase transformations during fast thermal transients, such as the ones that occur during welding, especially during heating, are virtually ignored.

Many phase transformations that occur during welding involve nucleation and growth phenomenon. In general, the phase transformation involves a change in the parent crystal structure to form the product phase. This crystal structure change can be brought about through atom motions by displacive or reconstructive mechanisms. In the former case, the change in crystal structure is achieved by the deformation of the parent phase. In the latter, the crystal structure change is achieved by random atom motions. For example, in steels, martensite phase formation from austenite occurs by a displacive mechanism, whereas the ferrite formation takes place by a reconstructive mechanism. Externally applied stresses, or residual stresses, which develop as a result of constraint in weldments, can influence the solid-state phase transformations in two ways. First, the stress can, in certain circumstances, provide a thermodynamic assist to the transformation or, conversely, can oppose it. Second, the stress can favor the growth of certain crystallographic variants. As a result, both the kinetics and appearance of the microstructure can be drastically affected (Bhadeshia, 1992).

One of the most exciting areas in welding research is the modeling of transformations in welds. The modeling involves a two-step process: first, a computational model that can accurately simulate the thermal history of the weld metal and the base plate must be developed, and, second, this thermal model needs to be coupled with an appropriate phase-transformation model. Such a coupled quantitative model would enable us to understand better the weld phase transformation characteristics and identify controlling variables. As discussed earlier in this article, significant efforts are under way using numerical

methods to calculate heat and mass transfer in welds. Limited efforts are also under way to develop appropriate models to characterize phase transformations in welds and predict microstructures (Henwood *et al.*, 1988; Watt *et al.*, 1988; Bhadeshia, 1990, 1992; Bhadeshia and Svensson, 1992; Easterling, 1992). Models based on physical metallurgy principles have been developed for a quantitative approach to predicting fusion-zone microstructures (Watt *et al.*, 1988). A coupled transient heat-transfer-microstructure weld model has also been developed for computing the heat-affected zone microstructures (Henwood *et al.*, 1988; Shen *et al.*, 1993). Recent work using the Monte Carlo technique has focussed on predicting microstructural features such as grain growth in a weld heat-affected zone (Shen *et al.*, 1993). Although the task at hand appears straightforward, the overall picture is complicated by a number of interacting factors, such as the welding process, that determine the pool shape and size, filler metal additions, material chemistry, solidification morphology, segregation, inclusion characteristics, grain size, welding speed and associated cooling rates, and multiple thermal cycles.

C. Residual stresses

One of the major concerns in welded structures is residual stresses and distortion. Due to localized heating, complex thermal and phase transformation stresses are generated during welding. In addition, thermal expansion and contraction of the solid during weld thermal cycles in a multipass weld also generate considerable thermal stresses and stress gradients that can exceed the yield strength of the materials. The residual stresses that develop in and around the welded joint are detrimental to the integrity and service life of the welded part. Residual stresses can lead to distortion, initiate fracture, and degrade corrosion resistance of the welded structural part (Welding Handbook, 1989).

Although residual stresses have been studied for many decades, accurate calculation and measurement of these stresses still remains a major issue. Computational models can provide a detailed description of the residual stress distribution in weldments (Hepworth, 1980; Ortega *et al.*, 1993; McDill *et al.*, 1993; Goldak, 1990; Mahin *et al.*, 1990; Tekriwal and Mazumder, 1990; Oddy *et al.*, 1990). A prerequisite for the calculations is the detailed and accurate time-temperature history obtained from numerical calculations. Calculations of distortions, stresses, and strains are computationally intensive, and they take significantly more computer time than the calculation of the transient temperature field. Recently, the trend in these calculations has moved from cross-sectional two-dimensional plane strain and axisymmetric models to models using plane stress, shell, and three-dimensional elements. Tekriwal and Mazumder (1990) performed a three-dimensional thermomechanical analysis of the gas-metal arc welding to calculate distortions, stresses, and strains. Good qualitative agreement was achieved between the calculated and the measured transient strains. However, the calculated and measured residual strains were different. The differences were attributed to lack of an accurate stress-strain constitutive relation and the use of a coarse grid. Oddy *et al.* (1990) showed that phase transformations can significantly affect the residual stresses generated by the welding of some steels. Thus the uncertainties in the calculation procedures include the inaccuracies in the calculation of transient time-temperature history as well as the approximations in the assumed stress-strain relation, particularly when important solid-state transformations take place.

Until the advent of neutron strain scanning, the characterization of residual stresses below the surface was limited to indirect and destructive methods such as hole drilling. Neutrons can penetrate easily into most materials, and now neutron diffraction is a well-established method for the measurement of residual stresses in metallic components. The method is nondestructive, in that the stress field in an object remains unperturbed by the measurement, and the level of induced radioactivity in the sample is usually negligible. Several residual stress measurements have been carried out on model single-pass and multipass welds in austenitic and ferritic steel welds (Allen *et al.*, 1985; Holden *et al.*, 1988; Mahin *et al.*, 1990; Root *et al.*, 1993a, 1993b; Spooner *et al.*, 1993) using neutron scattering. Application of this technique to three dimensional mapping of residual stresses in weldments has enormous potential in developing techniques to reduce or eliminate residual stresses in weldments.

VI. CONCLUDING REMARKS

In the last few decades, significant progress has been made in understanding welding processes and welded materials. However, several key problems and issues remain to be addressed. The main difficulties in the quantitative analysis of welding processes are the complexity of the physical processes in fusion welding and the scarcity of relevant data at very high temperatures, i.e., much higher than the melting point. In recent years, modeling has provided significant insight into the dynamics of the welding processes and the properties of the welded materials that could not have been obtained otherwise. However, modeling is computationally intensive, requires trained personnel, and is expensive. Although phenomenological modeling is a powerful tool, the modeling to date has been of limited practical use to practicing engineers because of the complexity, cost, and need for user training. Furthermore, most of the models have not been tested adequately, as the published works have focused on limited experimental verification. In view of the complexities of welding processes, theoretical calculations of welding variables must be tested by well-designed experiments. Reliable, science-based correlations between the microstructure and properties of welds, and models to predict such relations, are necessary for the development of the field. Moreover, because of the extreme cooling

conditions encountered during welding, the events that follow welding are far from equilibrium and, as a result, lead to the formation of nonequilibrium phases both in the fusion zone and heat-affected zone. Therefore modeling of phase transformations and the resulting microstructures in weldments remains a great challenge. Another key issue is the development of residual stress and stress gradients due to thermal effects and phase transformations encountered during welding. These effects significantly add to the complexities in understanding microstructure-property relationships and to the development of a capability to predict such relationships. Furthermore, compositional, microstructural, and stress gradients are unique to welded structures. The usual engineering mechanics treatment of material behavior assumes homogeneous properties. This approach is clearly not appropriate for weldments. A new opportunity exists for developing a theory and methodology to evaluating mechanical properties in the presence of various gradients.

Integration of a fundamental understanding of the welding processes and a knowledge of the evolution of microstructure and properties remains a major challenge in the pursuit of intelligent process control to produce defect-free, structurally sound, and reliable welds.

ACKNOWLEDGMENTS

The research was sponsored by the Division of Materials Sciences of the U.S. Department of Energy under Grant No. DE-FG02-84ER45158 with the Pennsylvania State University and Contract No. DE-AC05-84OR21400 with Martin Marietta Energy Systems, Inc. We thank Dr. S. Babu, Professor W. R. Bitler, Professor L. J. Cuddy, Professor T. W. Eagar, Mr. D. Madey, Professor J. Mazumder, Dr. K. Mundra, Mr. T. Palmer, and Dr. J. M. Vitek for their comments on the manuscript.

REFERENCES

Abdulgadar, S. A., 1988, Ph.D. thesis (Pennsylvania State University).

Allen, A. J., M. T. Hutchings, C. G. Windsor, and C. Andreani, 1985, Adv. Phys. **34**, 445.

American Welding Society Statement, 1992, USA Today, March 22, 1992.

Anderson, K., G. E. Cook, and R. J. Barnett, 1993, in *International Trends in Welding Science and Technology,* edited by S. A. David and J. Vitek [American Society for Metals (ASM) International, Materials Park, OH], p. 877.

Anisimov, S. I., and A. Kh. Rakhmatulina, 1973, Sov. Phys.-JETP **37**, 441.

Arata, Y., and I. Miyamoto, 1978, Technocrat **11** (5), 33.

Aziz, M. J., 1982, J. Appl. Phys. **53**, 1158.

Babu, S. S., S. A. David, J. M. Vitek, K. Mundra, and T. DebRoy, 1994, Mater. Sci. Tech. (in press).

Baker, J. C., 1970, Ph.D. thesis (Massachusetts Institute of Technology).

Bandopadhyay, A., A. Banerjee, and T. DebRoy, 1992, Metall. Trans. B **23B**, 207.

Banerjee, A., T. DebRoy, C. Onneby, and M. Small, 1993, in *International Trends in Welding Science and Technology,* edited by S. A. David and J. Vitek (ASM International, Materials Park, OH), p. 39.

Barr, W. L., 1962, J. Opt. Soc. Am. **52**, 885.

Basu, S., 1992, M.S. thesis (The Pennsylvania State University).

Basu, S., and T. DebRoy, 1992, J. Appl. Phys. **72**, 3317.

Batanov, V. A., F. V. Bunkin, A. M. Prokhorov, and V. B. Fedorov, 1973, Sov. Phys.-JETP **36**, 311.

Bennett, W. S., and G. S. Mills, 1974, Weld. J. Res. Suppl. **53**(12), 548s.

Bhadeshia, H. K. D. H., 1990, in *Recent Trends in Welding Science and Technology,* edited by S. A. David and J. M. Vitek (ASM International, Materials Park, Ohio), p. 189.

Bhadeshia, H. K. D. H, 1992, *Bainite in Steels* (Institute of Materials, London).

Bhadeshia, H. K. D. H, and L. E. Svensson, 1992, in *Mathematical Modeling of Weld Phenomena,* edited by H. Cerjak and K. E. Easterling (The Materials Society, London), p. 109.

Biloni, H., 1987, in *Physical Metallurgy,* Part I, edited by R. W. Cahn and P. Haasen (Elsevier, New York), p. 478.

Blake, A., and J. Mazumder, 1985, J. Eng. Ind. **107**, 275.

Block-Bolten, A., and T. W. Eager, 1982, in *Trends in Welding Research,* edited by S. A. David (ASM Publications, Metals Park, OH), p. 53.

Block-Bolten, A., and T. W. Eager, 1984, Metall. Trans. B **15**, p. 461.

Boettinger, W. J., and S. R. Coriell, 1984, Mater. Sci. Eng. **65**, 27.

Boumans, P. W. J. M., 1966, *Theory of Spectrochemical Excitation* (Hilger and Watts Ltd., London).

Brower, W. E., R. Strachan, and M. C. Flemings, 1970, AFS Cast Metals Research Journal **6**, (December), 176.

Bramson, M. A., 1968, *Infrared Radiation: A Handbook for Applications* (Plenum, New York).

Brody, H. D., and M. C. Flemings, 1966, Trans. AIME **236**, 615.

Brooks, J. A., and M. I. Baskes, 1986, in *Advances in Welding Science and Technology,* edited by S. A. David (ASM International, Metals Park, OH), p. 93.

Brooks, J. A., M. I. Baskes, and F. A. Greulich, 1991, Metall. Trans. A **22**, 915.

Cahn, J. W., S. R. Coriell, and W. J. Boettinger, 1979, in *Laser and Electron Beam Processing of Materials,* edited by C. W. White and P. S. Peercy (Materials Research Society, Pittsburgh, PA), p. 89.

Carslaw, H. S., and J. C. Jaegar, 1959, *Conduction of Heat in Solids* (Clarendon Press, Oxford).

Chai, C. S., and T. W. Eagar, 1980, Weld. J. **59** (3), 93s.

Chai, C. S., and T. W. Eagar, 1981, Metall. Trans. B. **12**, 539.

Chan, C., J. Mazumder, and M. M. Chen, 1984, Metall. Trans. A **15**, 2175.

Chan, C. L., and J. Mazumder, 1987, J. Appl. Phys. **62**, 4579.

Chennat, J., and C. Albright, 1985, in "Proceedings of the Materials Processing Symposium ICALEO, Boston, MA, November 1984," published in *Proceedings of the ICALEO,* Vol. 44, edited by J. Mazumder (The Laser Institute of America, Toledo, OH), p. 76.

Chun, M. K., and K. Rose, 1970, J. Appl. Phys. **41** (2), 614.

Choo, R. T., and J. Szekely, 1994, Weld. J. Res. Suppl. **73** (2), 25s.

Cieslak, M. J., 1991, in *Metal Science of Joining,* edited by M. J. Cieslak, J. H. Perepezko, S. Kang, and M. E. Glicksman (The

Minerals, Metals and Materials Society, Warrendale, PA), p. 101.
Cieslak, M. J., and P. W. Fuerschbach, 1988, Metall. Trans. B **19**, 319.
Collur, M. M., 1988, Ph.D. thesis (The Pennsylvania State University).
Collur, M. M., and T. DebRoy, 1989, Metall. Trans. B **20**, 227.
Collur, M. M., A. Paul, and T. DebRoy, 1987, Metall. Trans. B **18**, 733.
David, S. A., and T. DebRoy, 1992, Science **257**, 497.
David, S. A., T. DebRoy, and J. M. Vitek, 1994, MRS Bull. **19** (1), 29.
David, S. A., G. M. Goodwin, and D. N. Braski, 1979, Weld J. **58** (11), 330s.
David, S. A., and C. T. Liu, 1982, Weld. J. **61** (5), 157s.
David, S. A., and J. M. Vitek, 1982, in *Lasers in Metallurgy,* edited by K. Mukherjee and J. Mazumder (The Metallurgical Society of AIME, Warrendale, PA), p. 247.
David, S. A., and J. M. Vitek, 1989, Int. Mater. Rev. **34**, 213.
David, S. A., J. M. Vitek, and T. L. Hebble, 1987, Weld. J. **66** (10), 289s.
David, S. A., J. M. Vitek, M. Rappaz, and L. A. Boatner, 1990, Metall. Trans. A. **21**, 1753.
Davies, G. J., and J. G. Garland, 1975, Int. Met. Rev. **20**, 83.
DebRoy, T., 1993a, in *International Trends in Welding Science and Technology,* edited by S. A. David and J. Vitek (ASM International, Materials Park, OH), p. 17.
DebRoy, T., 1993b, Paper presented at the 2nd International Seminar on Numerical Analysis on Weldability, 10–11 May, Graz-Seggau, Austria, unpublished.
DebRoy, T., S. Basu, and K. Mundra, 1991, J. Appl. Phys. **70**, 1313.
den Ouden, G., and O. Griebling, 1990, in *Recent Trends in Welding Science and Technology,* edited by S. A. David and J. M. Vitek (ASM International, Materials Park, OH), p. 431.
Dixon, R. D., and G. K. Lewis, 1985, in "Proceedings of the Materials Processing Symposium ICALEO, Boston, MA, November 1984," published in *Proceedings of the ICALEO,* Vol. 44, edited by J. Mazumder (The Laser Institute of America, Toledo, OH), p. 28.
Dowden, J., M. Davis, and P. Kapadia, 1985, J. Appl. Phys. **57** (9), 4474.
Dunn, G. J., C. D. Allemand, and T. W. Eagar, 1986, Metall. Trans. A **17**, 1851.
Dunn, G. J., and T. W. Eagar, 1986, Metall. Trans. A **17**, 1865.
Dushman, S., 1962, *Scientific Foundations of Vacuum Technique,* Second ed. (Wiley, New York).
Duwez, P., P. H. Willens, and W. Klement, 1960, Nature **187**, 69.
Easterling, K. E., 1992, in *Mathematical Modeling of Weld Phenomena,* edited by H. Cerjak and K. E. Easterling (The Materials Society, London), p. 163.
Elliott, J. F., and M. Gleiser, 1960, *Thermochemistry for Steelmaking,* Vol. I (Addison Wesley, Reading, MA).
Elliott, J. F., M. Gleiser, and V. Ramakrishna, 1963, *Thermochemistry for Steelmaking,* Vol. II (Addison Wesley, Reading, MA).
Elmer, J. W., S. M. Allen, and T. W. Eagar, 1989, Metall. Trans. A. **20**, 2117.
Flemings, M. C., 1974, *Solidification Processing* (McGraw-Hill, New York).
Frost, R. H., D. L. Olson, and S. Liu, 1993, in *International Trends in Welding Science and Technology,* edited by S. A. David and J. Vitek (ASM International, Materials Park, OH), p. 205.
Fuerschbach, P. W., 1994, "Measurement and Prediction of Energy Transfer Efficiency in Laser Beam Welding," private communication, Sandia National Laboratory.
Fuerschbach, P. W., and G. A. Knorovsky, 1991, Weld. J. Res. Suppl. **70** (10), 287s.
Garland, G. J., 1972, Ph.D. thesis (University of Cambridge, UK).
Geankoplis, C. J., 1983, *Transport Processes and Unit Operations* (Allyn and Bacon, Boston), p. 186.
Gedeon, S. A., and T. W. Eagar, 1990, Weld. J. Res. Suppl. **69**, 264s.
Giedt, W. H., L. N. Tallerico, and P. W. Fuerschbach, 1989, Weld. J. Res. Suppl. **68** (1), 28s.
Glicksman, M. E., 1989, in *Principles of Solidification and Materials Processing,* Vol. I, edited by R. Trivedi, J. A. Sekhar, and J. Mazumder (Oxford & IBH, Publishing Co. Pvt., Ltd., New Delhi), p. 11.
Glickstein, S. S., 1976, Weld. J. Res. Suppl. **55** (8), 222s.
Goldak, J., 1990, in *Recent Trends in Welding Research,* edited by S. A. David and J. M. Vitek (ASM International, Materials Park, OH), p. 71.
Griem, H. R., 1964, *Plasma Spectroscopy* (McGraw-Hill, New York).
Griem, H. R., 1974, *Spectral Line Broadening by Plasmas* (Academic, New York).
Heald, M. A., and C. B. Wharton, 1965, *Plasma Diagnostics with Microwaves* (Wiley, New York).
Heiple, C. R., and J. R. Roper, 1982a, Weld. J. Res. Suppl. **61**, 97s.
Heiple, C. R., and J. R. Roper, 1982b, in *Trends in Welding Research,* edited by S. A. David (ASM, Metals Park, OH), p. 489.
Heiple, C. R., J. R. Roper, R. T. Stagner, and J. J. Alden, 1982, Weld. J. Res. Suppl. **61**, 72s.
Henwood, C., M. Bibby, J. Goldak, and D. Watt, 1988, Acta Metall. **36** (11), 3037.
Hepworth, J. K., 1980, in *Finite Element Calculation of Residual Stresses in Welds,* Proceedings of International Conference on Numerical Methods for Non-Linear Problems, September 1980 (Pineridge Prep, Swansea, Wales), p. 51.
Holden, T. M., J. H. Root, V. Fidleris, R. A. Holt, and G. Roy, 1988, Mater. Sci. Forum **27** and **28**, 359.
Huntington, C. A., and T. W. Eagar, 1983, Weld. J. Res. Suppl. **62** (4), 105s.
Indacochea, J. E., M. Blander, N. Christensen, and D. L. Olson, 1985, Metall. Trans. B. **16**, 237.
Jackson, K. A., G. H. Gilmer, and H. J. Leamy, 1979, in *Laser and Electron Beam Processing of Materials,* edited by C. W. White and P. S. Peercy (Materials Research Society, Pittsburgh, PA), p. 104.
Katayama, S., and A. Matsunawa, 1985, in "Proceedings of the Materials Processing Symposium ICALEO, Boston, MA, November 1984," published in *Proceedings of the ICALEO,* Vol. 44, edited by J. Mazumder (The Laser Institute of America, Toledo, OH), p. 60.
Katayama, S., and A. Matsunawa, 1986, in "Proceedings of the International Conference on Applications of Lasers and Electro-optics, San Francisco, CA, November 1985," published in *Laser Welding, Machining and Materials Processing,* edited by C. Albright (Springer-Verlag, Berlin), p. 19.
Kerr, H. W, and J. C. Villafuerte, 1992, in *The Metal Science of Joining,* edited by M. J. Cieslak, J. H. Perepezko, S. Kang, and M. E. Glicksman (The Minerals, Metals and Materials Society,

Warrendale, PA), p. 11.
Key, J. F., J. W. Chan, and M. E. McIlwain, 1983, Weld. J. Res. Suppl. **62** (7), 179s.
Key, J. F., M. E. McIlwain, and L. Isaacson, 1980, in *Sixth International Conference on Gas Discharges and their Applications,* Riccarton, UK, No. 189, Part 2 (Institution of Electrical Engineers, New York), p. 235.
Khan, P. A. A., 1987, Ph.D. thesis (The Pennsylvania State University).
Khan, P. A. A., and T. DebRoy, 1984, Metall. Trans. B **15**, 641.
Khan, P. A. A., and T. DebRoy, 1985, Metall. Trans. B **16**, 853.
Khan, P. A. A., T. DebRoy, and S. A. David, 1988, Weld. J. Res. Suppl. **67**, 1s.
Kluken, A. O., and Ø. Grong, 1989, Metall. Trans. A **20**, 1335.
Knight, C. J., 1979, AIAA J. **17**, 519.
Knudtsen, J. T., W. B. Green, and D. G. Sutton, 1987, J. Appl. Phys. **61** (10), 4771.
Kou, S., 1987, *Welding Metallurgy* (John Wiley and Sons, New York).
Kou, S., and Y. Le, 1983, Metall. Trans. A **14**, 2245.
Kraus, H. G., 1989, Weld. J. Res. Suppl. **68**, 269s.
Kurz, W., and W. Clyne, 1981, Metall. Trans. A **12**, 965.
Kurz, W., and D. J. Fisher, 1981, Acta Metall. **29**, 11.
Kurz, W., and D. J. Fisher, 1986, *Fundamentals of Solidification* (Trans. Tech. Publications, Aedermannsdorf, Switzerland).
Kurz, W., B. Giovanola, and R. Trivedi, 1986, Acta Metall. **34**, 823.
Kurz, W., and R. Trivedi, 1989, in *Principles of Solidification and Materials Processing,* Vol. 1, edited by R. Trivedi, J. A. Sekhar, and J. Mazumder (Oxford & IBH Publishing Co., Pvt., Ltd., New Delhi), p. 67.
Lancaster, J. F., 1980, *Metallurgy of Welding* (Allen and Unwin, London).
Langer, J. S., 1989, in *Principles of Solidification and Materials Processing,* Vol. I, edited by R. Trivedi, J. A. Sekhar, and J. Mazumder (Oxford & IBH Pvt. Ltd., New Delhi), p. 1.
Langer, J. S., and H. Muller-Krumbhaar, 1987, Acta Metall. **26**, 1681.
Lin, W., J. Lippold, and W. A. Baeslack III, 1993, Weld. J. Res. Suppl. **72** (4), 165s.
Lippold, J. C., 1994, Weld. J. Res. Suppl. **73**, 129s.
Mahin, K. W., W. Winters, J. Krafcik, T. Holden, R. Hosbons, and S. MacEwen, 1990, in *International Trends in Welding Science and Technology,* edited by S. A. David and J. M. Vitek (ASM International, Materials Park, OH), p. 83.
Matsuda, F., T. Hashimato, and T. Senda, 1969, Trans. Natl. Res. Inst. Met. (Jpn) **11** (1), 43.
Matsunawa, A., 1993, in *International Trends in Welding Science and Technology,* edited by S. A. David, and J. Vitek (ASM International, Materials Park, OH), p. 3.
Mazumder, J. 1993, ASM Handbook, ASM International, Materials Park, OH, **6**, 1146.
Mazumder, J., and A. Kar, 1992, in *Thermomechanical Aspects of Manufacturing and Materials Processing,* edited by R. K. Shah *et al.* (Hemisphere, New York), p. 283.
McDill, J. M. J., A. S. Oddy, and J. A. Goldak, 1993, in *International Trends in Welding Science and Technology,* edited by S. A. David and J. M. Vitek (ASM International, Materials Park, OH), p. 105.
McNallan, M. J., and T. DebRoy, 1991, Metall. Trans. B **22**, 557.
Mehrabian, R., 1982, Int. Met. Rev. **27**, 185.
Metcalfe, J. C., and M. B. C. Quigley, 1977, Weld. J. Res. Suppl. **56** (5), 133s.
Metzbower, E. A., 1993, Metall. Trans. B **24**, 875.
Miller, R., 1989, *Absorption of Laser Beam by Plasma During Laser Welding of Stainless Steel,* M.S. thesis (The Pennsylvania State University).
Miller, R., and T. DebRoy, 1990, J. Appl. Phys. **68** (5), 2045.
Mills, G. S., 1977, Weld. J. Res. Suppl. **56**, 186s.
Mitra, U., and T. W. Eagar, 1991a, Metall. Trans. B **22**, 65.
Mitra, U., and T. W. Eagar, 1991b, Metall. Trans. B **22**, 73.
Mitra, U., and T. W. Eagar, 1991c, Metall. Trans. B **22**, 83.
Mullins, W. W., and R. F. Sekerka, 1964, J. Appl. Phys. **35**, 444.
Mundra, K., and T. DebRoy, 1993a, unpublished research, conducted at Department of Materials Science and Engineering, The Pennsylvania State University, University Park, PA.
Mundra, K., and T. DebRoy, 1993b, Metall. Trans. B **24**, 145.
Mundra, K., and T. DebRoy, 1993c, Weld. J. Res. Suppl. **72**, 1s.
Nippes, E. F., W. F. Savage, and G. Grotke, 1957, Weld. Res. Council. Bull. **33**, 1.
Nippes, E. F., H. Wawrousek, and W. L. Fleishman, 1955, Weld. J. **34**, 169s.
Oddy, A. S., J. A. Goldak, and J. M. J. McDill, 1990, in *International Trends in Welding Science and Technology,* edited by S. A. David and J. M. Vitek (ASM International, Materials Park, OH), p. 97.
Ohno, S., and M. Uda, 1981, Trans. Natl. Res. Inst. Met. (Jpn.) **23**, 243.
Oreper, G. M., and J. Szekely, 1984, J. Fluid Mech. **147**, 53.
Ortega, A. R., L. A. Bertram, E. A. Fuchs, K. Mahin, and D. V. Nelson, 1993, in *International Trends in Welding Science and Technology,* edited by S. A. David and J. M. Vitek (ASM International, Materials Park, OH), p. 89.
Patterson, R. A., and K. W. Mahin, 1990, Eds., *Weldability of Materials,* Proceedings of Materials Weldability Symposium, Detroit, MI, 8–12 October, 1990 (ASM International, Materials Park, OH).
Paul, A., and T. DebRoy, 1986, in *Advances in Welding Science and Technology,* edited by S. A. David (ASM, Materials Park, OH), p. 29.
Paul, A. J., and T. DebRoy, 1988, Metall. Trans. B **19**, 851.
Peebles, H. C., and R. L. Williamson, 1987, in Proceedings of International Conference on Laser Advanced Materials Processing—Science and Application, Osaka, Japan, May 1987 (High Temperature Society of Japan, Osaka, Japan), p. 19.
Pehlke R. D., 1979, *Unit Processes in Extractive Metallurgy* (Elsevier, New York).
Pehlke R. D., and J. F. Elliott, 1960, Trans. Metall. Soc. AIME **218**, 1091.
Rappaz, M., B. Carrupt, M. Zimmerman, and W. Kurz, 1987, Helv. Phys. Acta. **60**, 924.
Rappaz, M., S. A. David, J. M. Vitek, and L. A. Boatner, 1989, Metall. Trans. A **20**, 1125.
Rappaz, M., S. A. David, J. M. Vitek, and L. A. Boatner, 1990, Metall. Trans. A **21**, 1767.
Rappaz, M., M. Gremaud, R. Dekumbis, and W. Kurz, 1987, in *Laser Treatment of Materials,* edited by B. J. Mordike (DGM Informationsgesellschaftverlag, Bad Nauheim, FRG).
Richardson, F. D., 1974, *Physical Chemistry of Melts in Metallurgy,* Vol. 2 (Academic, London), p. 349.
Rockstroh, T. D., 1987, Ph.D. thesis (University of Illinois at Urbana-Champaign).
Rockstroh, T. D., and J. Mazumder, 1987, J. Appl. Phys. **61** (3), 917.
Root, J. H., T. M. Holden, J. Schroder, C. A. Hubbard, S.

Spooner, T. A. Dodson, and S. A. David, 1993a, Mater. Sci. Technol. **9**, 754.

Root, J. H., T. M. Holden, J. Schroder, S. Spooner, C. A. Hubbard, T. A. Dodson, and S. A. David, 1993b, in *International Trends in Welding Science and Technology,* edited by S. A. David and J. M. Vitek (ASM International, Materials Park, OH), p. 99.

Sahoo, P., M. M. Collur, and T. DebRoy, 1988, Metall. Trans. B **18**, 967.

Sahoo, P., and T. DebRoy, 1987, Metall. Trans. B **18**, 597.

Sahoo, P., T. DebRoy, and M. J. McNallan, 1988, Metall. Trans. B **19**, 483.

Savage, W. F., 1980, Weld. World **18**, 89.

Scheil, E., 1942, Z. Metall. **34**, 70.

Shaw, C. B., Jr., 1975, Weld. J. Res. Suppl. **54** (2), 33s.

Shen, Y., B. Radhakrishnan, and R. G. Thompson, 1993, in *International Trends in Welding Science and Technology,* edited by S. A. David and J. M. Vitek (ASM International, Materials Park, OH), p. 259.

Smartt, H. B., J. A. Stewart, and C. J. Einerson, 1985, ASM Metals/Technology Series, paper #8511/011 (ASM, Metals Park, OH).

Spooner, S., T. M. Holden, J. H. Root, and S. A. David, 1993, in *Trends in Welding Research,* edited by S. A. David and J. M. Vitek (ASM International, Materials Park, OH, 1993), p. 139.

Steeb, S., and H. Warlimont, 1985, Eds., Proc. 5th Int. Conf. on Rapidly Quenched Metals (North-Holland Physics, Amsterdam).

Szekely, J., 1986, in *Advances in Welding Science and Technology,* edited by S. A. David (ASM International, Materials Park, OH), p. 3.

Tekriwal P., and J. Mazumder, 1990, in *International Trends in Welding Science and Technology,* edited by S. A. David and J. M. Vitek (ASM International, Materials Park, OH), p. 91.

Trivedi, R., 1970, Acta Metall. **18**, 287.

Trivedi, R., and W. Kurz, 1986, Acta Metall. **34**, 1663.

Tsai, M. C., and S. Kou, 1989, J. Numer. Methods Phys. **9**, 1503.

Uda, M., S. Ohno, and T. Wada, 1969, J. Jpn. Weld. Soc. **38**, 382.

Uda, M., and S. Ohno, 1973, Trans. Natl. Res. Inst. Met. **15**, 20.

Venkataraman, S., and J. H. Devletian, 1988, Weld. J. **67** (6), 111s.

Vitek, J. M., A. Das Gupta, and S. A. David, 1983, Metall. Trans. A **14**, 1933.

Vitek, J. M., and S. A. David, 1990, in *First U.S.–Japan Symposium on Advances in Welding Metallurgy,* June 7 to 8, 1990 (American Welding Society and Japan Welding Society, Japan Welding Engineering Society, San Francisco), p. 65.

Vitek, J. M., S. A. David, L. A. Boatner, and M. Rappaz, 1993, in *International Trends in Welding Science and Technology,* edited by S. A. David and J. M. Vitek (ASM International, Materials Park, OH), p. 167.

von Allmen, M., 1976, J. Appl. Phys. **47**, 5460.

von Allmen M., 1987, *Laser-Beam Interactions with Materials* (Springer-Verlag, Berlin).

Wang, Y. H., and S. Kou, 1986, in *Advances in Welding Science and Technology,* edited by S. A. David (ASM International, Materials Park, OH), p. 65.

Watt, D. F., L. Coon, M. Bibby, J. Goldak, and C. Henwood, 1988, Acta Metall. **36** (11), 3029.

Welding Handbook, 1989, 8th ed., Chap. 7, prepared by a committee consisting of K. Masubuchi, O. W. Blodgett, S. Matsui, F. P. Ross, C. O. Rudd, and C. L. Tsai (American Welding Society, Miami, FL).

White, D. R., J. A. Carmein, J. E. Jones, and K. Liu, 1993, in *International Trends in Welding Science and Technology,* edited by S. A. David and J. Vitek (ASM International, Materials Park, OH), p. 883.

Wood, R. F., 1982, Phys. Rev. B. **25**, 2786.

Woods, R. A., and Milner, D. R., 1971, Weld. J. Res. Suppl. **50**, 163s.

Zacharia, T., S. A. David, J. M. Vitek, and T. DebRoy, 1989a, Weld. J. Res. Suppl. **68**, 510s.

Zacharia, T., S. A. David, J. M. Vitek, and T. DebRoy, 1989b, Metall. Trans. A **20**, 957.

ZelDovich Y. B., and Y. P. Raizer, 1966, *Physics of Shock Waves and High Temperature Hydrodynamic Phenomena* (Academic, New York).

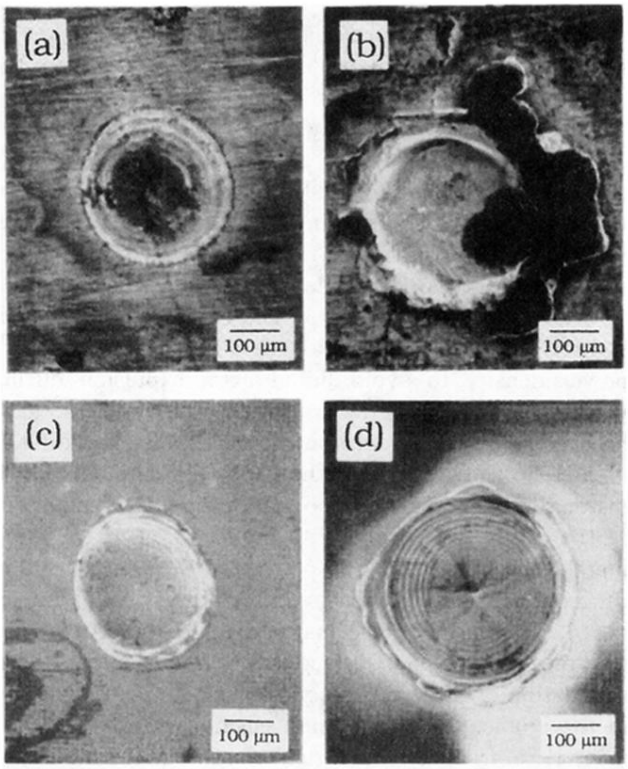

FIG. 13. Micrographs of lead and stainless-steel samples irradiated by laser pulses of increasing duration leading to liquid expulsion. Lead irradiated by single pulses of (a) 0.05 and (b) 0.10 ms durations. Stainless steel irradiated by single pulses of (c) 0.5 and (d) 1.0 ms durations. Laser power, 500 W (Basu and DebRoy, 1992).

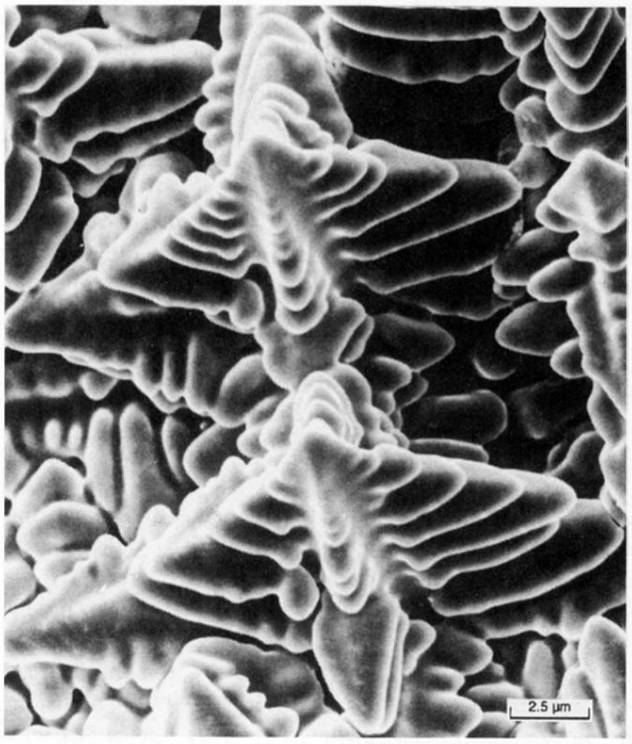

FIG. 26. Scanning electron micrograph showing the development of dendrites in a nickels-based superalloy single-crystal electron beam weld. The primary, secondary, and tertiary dendritic arms are clearly discernible (David and DebRoy, 1992).

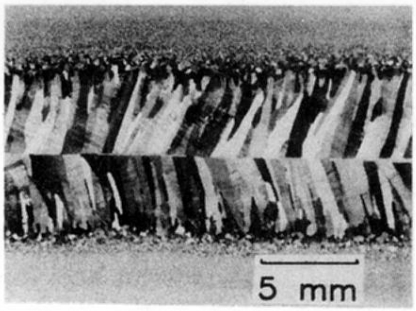

FIG. 29. Columnar grain structure in a steel weld (Courtesy of H. W. Kerr, University of Waterloo, Waterloo, Canada).

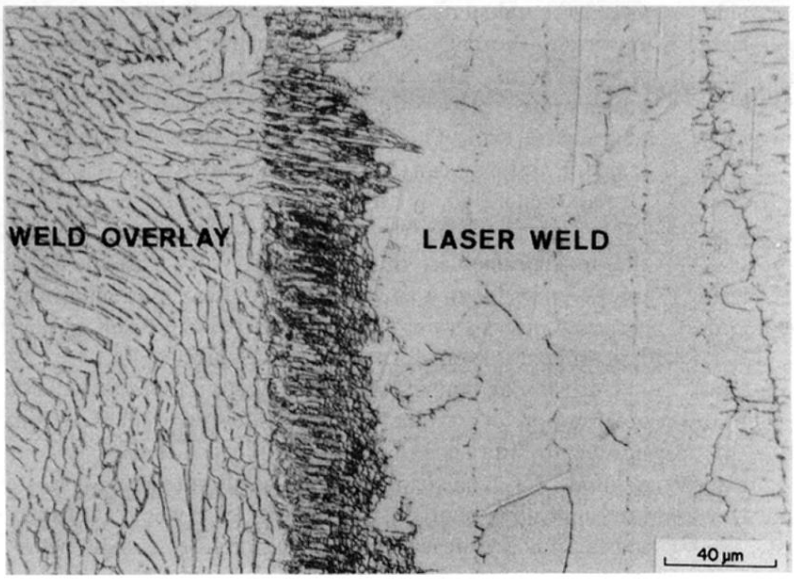

FIG. 31. Duplex (austenite and ferrite) structure modified by laser welding to produce a fully austenite structure (David and Vitek, 1982).